THE DYNAMICS AND EXCHANGE FLOW VARIABILITY OF THE COOS ESTUARY

by

TED B. CONROY

A THESIS

Presented to the Department of Earth Sciences
and the Graduate School of the University of Oregon
in partial fulfillment of the requirements
for the degree of
Master of Science

September 2018

THESIS APPROVAL PAGE

Student: Ted B. Conroy

Title: The Dynamics and Exchange Flow Variability of the Coos Estuary

This thesis has been accepted and approved in partial fulfillment of the requirements for the Master of Science degree in the Department of Earth Sciences by:

Alan W. Rempel	Chair
David A. Sutherland	Advisor
David K. Ralston	Member
Joshua J. Roering	Member

and

Janet Woodruff-Borden	Vice Provost and Dean of the Graduate School

Original approval signatures are on file with the University of Oregon Graduate School.

Degree awarded September 2018

THESIS ABSTRACT

Ted B. Conroy

Master of Science

Department of Earth Sciences

September 2018

Title: The Dynamics and Exchange Flow Variability of the Coos Estuary

Many estuaries have large variability in salinity structure due to variable river discharge, having the potential to induce large seasonal changes in estuarine exchange flow. In this study, a numerical ocean model of the Coos Estuary, Oregon, is developed and used to examine the variability of the estuarine exchange flow. The exchange flow is driven by tidal processes and is strongly modified by the strength of the tidal forcing: a higher exchange of volume and salt occurs during the larger amplitude fortnightly spring tides. This forcing maintains a persistent exchange flow with constant periodicity year-round, although the hydrography of the estuary is highly seasonal. The geometry of the estuary, composed of a dredged main channel and multiple connecting tributaries, significantly influences the dynamics of the estuary, including the length of the salinity intrusion, the importance of tidal timescale correlations between velocity and salinity, and freshwater advection throughout the estuary.

CURRICULUM VITAE

NAME OF AUTHOR: Ted B. Conroy

GRADUATE AND UNDERGRADUATE SCHOOLS ATTENDED:

University of Oregon, Eugene, OR, USA
University of Hawaii at Manoa, Honolulu, HI, USA

DEGREES AWARDED:

Master of Science, Earth Sciences, 2018, University of Oregon
Bachelor of Science, Global Environmental Science, 2015, University of Hawaii at Manoa

AREAS OF SPECIAL INTEREST:

Physical Oceanography
Estuarine Physics
Coastal Processes

PROFESSIONAL EXPERIENCE:

Graduate Employee, Department of Earth Sciences, University of Oregon, 2016 - 2018
Lab Technician, Analytical Geochemistry Lab, University of Hawaii at Manoa, 2014-2015

GRANTS, AWARDS AND HONORS:

Thayer Environmental Award, Department of Earth Sciences, University of Oregon, 2017

PUBLICATIONS:

Conroy, T, B., & Sutherland, D. A., & D. K. Ralston. Estuarine exchange flow variability in a Pacific Northwest estuary. "in preparation".

ACKNOWLEDGEMENTS

Thank you to David Sutherland for mentoring me throughout the project and introducing me to the wonderful world of estuarine physics. The oceanography group at the University of Oregon constantly provided support and a terrific work environment. Thank you to David Ralston for the mentoring and advice throughout the two years. Thank you to Dustin Carroll, who took me surfing as well as always offered positive support. Finally, thank you to my family and friends!

TABLE OF CONTENTS

LIST OF FIGURES

LIST OF TABLES

Table Page

CHAPTER I

INTRODUCTION

The salinity and velocity structure of an estuary is dependent on the tidal forcing, freshwater input, and the bathymetry and geometry of the basin. The river flux expels salt from the basin, and creates an along estuary baroclinic pressure gradient. The baroclinic pressure gradient, in addition to mixing caused by tidal currents, leads to a down-gradient transport of salt into the estuary (Lerczak et al., 2006). Estuarine exchange flow, the subtidal (i.e. tidally averaged) inflowing and outflowing volume flux, is an important diagnostic for the flushing of an estuary, as it is responsible for the transport of water parcels, nutrients, organisms, and pollutants through an estuary (MacCready and Banas, 2010) on timescales longer than a tidal cycle. Exchange flow is defined using the coupled time dependent conservation of volume and salt within an estuary (Knudsen, 1900; Burchard et al., 2018), resulting in inflowing and outflowing parcels of differing salinity due to turbulent mixing within the estuary (Wang et al., 2017).

Classic estuarine theory attributes the exchange flow to gravitational circulation; a steady balance between the along channel pressure gradient and vertical stress divergence (Pritchard, 1956; Hansen and Rattray, 1965). However, numerous other processes have been shown to contribute to exchange flow at subtidal frequencies (Geyer and MacCready, 2014), as any process that is not symmetric between the flood and ebb tide would be seen in the tidally averaged fields. Because of this, tidally averaged fields may be recording a complex blend of processes, such as gravitational circulation in addition to tidal straining (Simpson et al., 1990) or advective accelerations (Lerczak et al., 2004, Scully et al., 2009). Furthermore, in many estuaries, the tidal timescale correlation of salinity and

velocity may be a significant contribution to the total salt flux, relative to the subtidal flux. The mechanisms for salt fluxes at tidal timescales are difficult to distinguish (Chen et al., 2012), and are dependent on the geometry and flow characteristics of a specific estuary (Fischer, 1976). Recently, MacCready (2011) proposed the Total Exchange Flow (TEF) method, an isohaline quantification of salt and volume fluxes that exactly satisfies the above definition of the estuarine exchange flow. The TEF method combines all fluxes at tidal and subtidal frequencies, illustrating that processes occurring at tidal timescales can contribute significantly to the exchange flow, depending on the geometry and forcing on a particular estuary (Chen et al., 2012).

Estuaries in the U.S. Pacific Northwest (PNW) have strong tidal forcing and highly seasonal river discharge, driven by episodic storm events occurring from the fall to spring. Summer precipitation is rare and freshwater input decreases substantially, dramatically changing the along channel salinity gradient in small to mid-size estuaries (Banas et al., 2004, Sutherland and O'Neil, 2016). Shelf processes associated with the seasonal and synoptic time scale variability of along coast winds and the California Current System result in varying water properties and sea level height at the ocean-estuary boundary (Hickey and Banas, 2003). During the dry season, corresponding with upwelling events, water masses with low dissolved oxygen, which can be further depleted by respiration occurring within the estuary (O'Higgins and Rumrill, 2008), and high nutrient levels can propagate into estuarine waters (Roegner et al., 2011). The time scale of exchange between an estuary and the coastal ocean has important implications for larval recruitment within an estuary (Peteiro and Shanks, 2015; Banas et al., 2009). Nutrient import from the coastal ocean, rather than terrestrial runoff, is the main

supply for primary production in PNW estuaries (Roegner and Shanks, 2001). Thus, the seasonal magnitude of estuarine exchange flow has important biological implications, and more generally, it is of interest which mechanisms are driving the exchange flow and how an estuary responds to environmental forcing.

Studies of estuarine dynamics in the region have noted the importance of tidal processes for driving exchange in PNW estuaries. For example, Banas et al. (2004) showed that upstream salt fluxes in Willapa Bay, WA, were largely attributed to lateral tidal stirring, providing a high baseline exchange with smaller seasonal variability associated with river discharge. However, the dynamics of smaller estuaries in the region have not been investigated as thoroughly as the larger estuaries. These estuaries are typically short (i.e. length of salt intrusion) and their tidal prism is large relative to estuaries on the U.S. East Coast (Hickey and Banas, 2003). The exchange flow dynamics of short estuaries is complicated by the large modulation of the salinity and velocity field during the tidal cycle (Ralston et al., 2010), and the relevance of classic estuarine theory for these systems is unclear (e.g. Chen et al., 2012). Furthermore, many estuaries have a complex geometry, with multiple freshwater inputs and large bathymetric variability, either naturally occurring or due to dredging.

In this study, we describe the seasonal variation in hydrography, salt fluxes, and estuarine exchange flow of the Coos Estuary, Oregon, using observations and a numerical ocean model. Due to the large seasonal changes in hydrography and the along channel salinity gradient (roughly 1.5 to 0.15 $\frac{psu}{km}$), we expect large changes in the exchange flow seasonally, as the strength of the gravitational circulation, as well as tidal timescale diffusive fluxes, scale with the magnitude of the along channel salinity gradient. Seasonal variation in subtidal along channel

velocity was seen in Elkhorn Slough, a smaller West coast estuary (Nidzieko and Monismith, 2012). Similar seasonal variability in the magnitude of subtidal currents in the Coos Estuary is found. However, by using the isohaline TEF method, we find that the strong tidal forcing is the main driver of the exchange flow, which maintains a consistent exchange flow year round, and that the dominant time scale of variability is the fortnightly spring-neap cycle. The geometry, including multiple connected tributaries with freshwater inputs, and large bathymetric variability of the estuary lead to complex circulation and transport patterns within the estuary, and ultimately dictate the variability of the exchange flow.

CHAPTER II

BACKGROUND

The Coos Estuary (Fig. 1) is the second largest estuary in Oregon after the Columbia River Estuary, in terms of surface area (34 km^2) and volume (0.14 km^3) (Hickey and Banas, 2003). Due to the dredged main channel, the tidal prism in the Coos (30%) is reduced relative to smaller Oregon estuaries (typically 50%), but is larger than the Columbia River Estuary (14%) (Hickey and Banas, 2003). Jetties flank the entrance to the estuary, which is composed of a sinuous, dredged main channel and multiple shallower connecting channels. From the mouth the depth transitions into a deeper area (20 m depth at 3 km from the mouth, Fig. 2a) into the narrow dredged channel (dredged to 13 meters depth, and 91 meters wide), which has a steep, rectangular cross-sectional shape flanked by shoals and tidal flats. The dredged channel continues past the town of Coos Bay (km 23) and ends in Isthmus Slough, which is the deepest of all the Sloughs connecting to the estuary. Large bathymetric gradients exist due to the dredging (Fig. 2a.), including from the main channel to South Slough as well as from the main channel to Marshfield Channel where the Coos River enters the estuary (Fig. 1).

Most ($\sim$ 85%) of the freshwater is input by the Coos River, which enters the estuary through Marshfield Channel and the East Bay tidal flats. Discharge is highly seasonal and episodic (Fig. 3), with typical discharge events from the Coos River of 50-500 m^3s^{-1} occurring on synoptic timescales, and background winter flows of 10-50 m^3s^{-1}, similar to or smaller than many of the smaller estuaries in Oregon. During the summer discharge from the Coos River falls to 1-2 m^3s^{-1}. Many other creeks and rivers enter the estuary, such as Winchester Creek (Fig. 1), which has been gauged previously, where peak winter discharge events are 1-

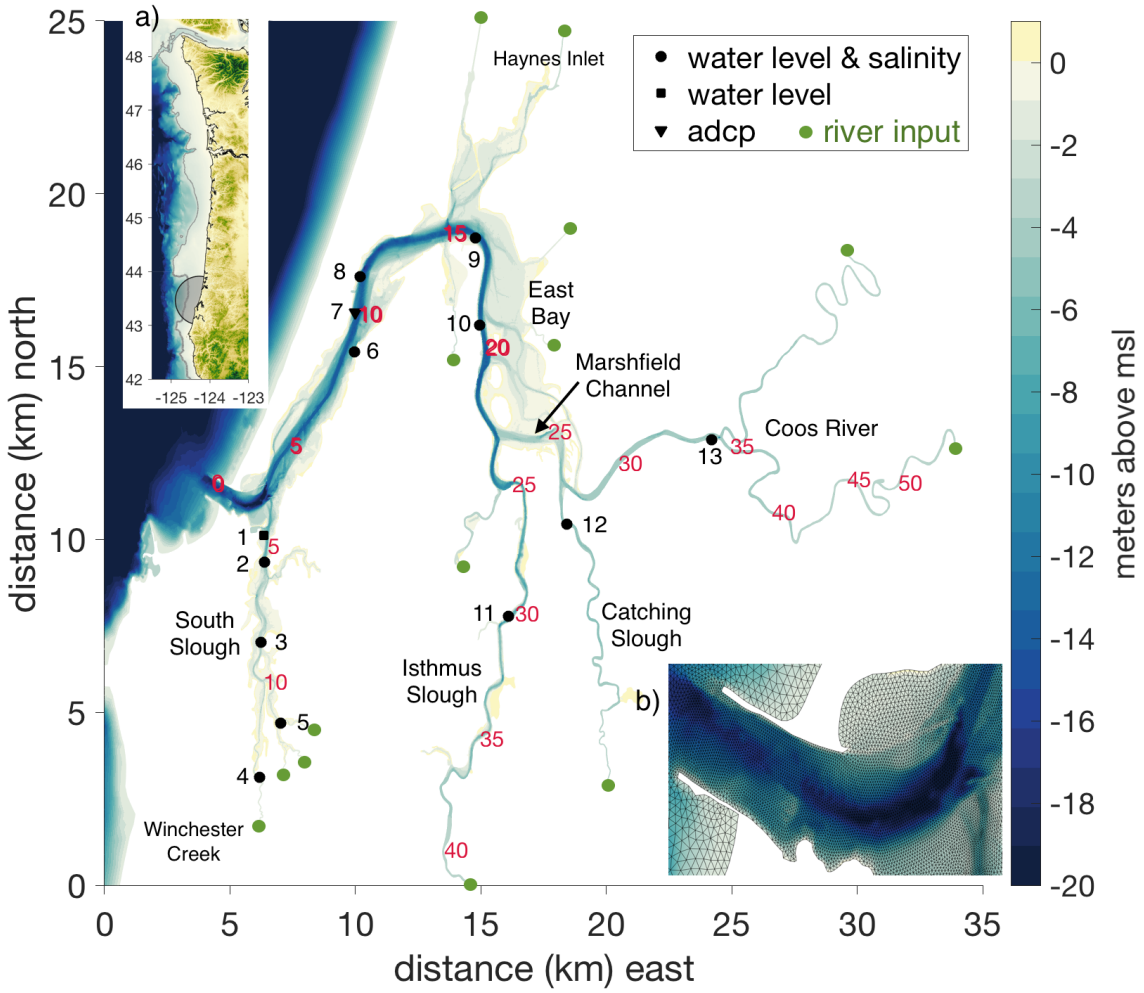

Figure 1. Bathymetry map of the Pacific NorthWest and numerical model domain of the Coos Estuary.
a) Elevation map of the U.S. Pacific Northwest coastline. The shelf break (-200 meter contour) is shaded in gray, and the numerical model domain is shown in the black outline. The main figure shows the bathymetry map and numerical model domain of the Coos Estuary, in meters above mean sea level. The red labels correspond to distance (in km) from the mouth of the estuary along the thalweg. The observational stations are labeled numerically on the map, and the corresponding names of the stations are found in Table 1. Major geographical locations are labeled. b) shows the unstructured numerical model grid at the mouth of the estuary.

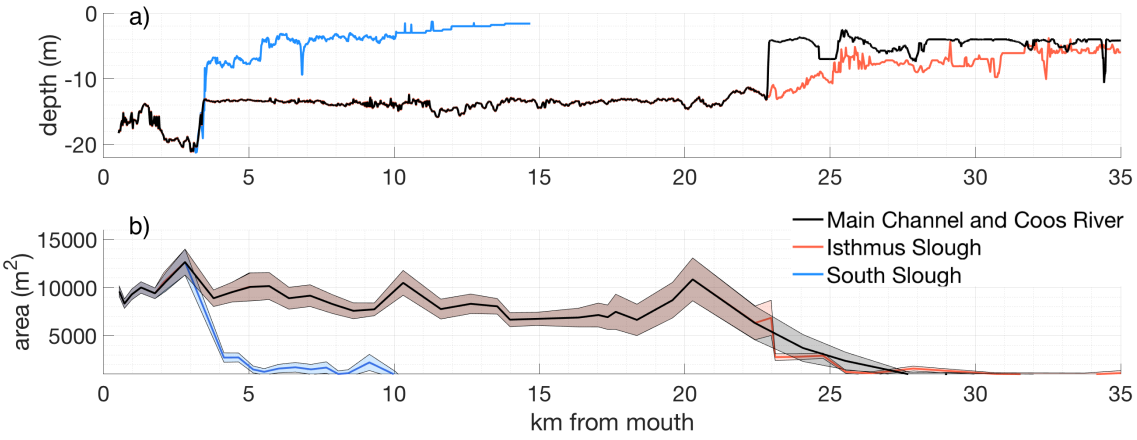

Figure 2. Thalweg depth and cross sectional area of the major channels of the estuary.
a) Depth of the thalweg up the Coos River, Isthmus Slough, and South Slough (meters above mean sea level). b) Cross sectional areas (m^2) of channels in a); the solid line is the mean area, and the shaded area is one standard deviation from the mean, representing tidal variation in cross sectional area.

3 m^3s^{-1}. The tides are mixed semidiurnal, having one strong ebb and flood each day. The mean tidal range is 1.7 m and the mean diurnal range is 2.3 m, and the spring-neap amplitude difference is typically 1.5 m. Tidal currents are O(1 ms^{-1}), and are greatest during ebb tides. Tidal excursions vary throughout the estuary, but are roughly 10-15 km in the main channel. The partially progressive tide wave propagates approximately 60 km up the Coos River, and reaches the full extent of the smaller channels. The salinity intrusion varies substantially annually, ranging from 23 to 50 km up the estuary.

Sutherland and O'Neill (2016) characterized the hydrographic structure of the estuary throughout 2012-2014, documenting the salinity structure transition from vertically well mixed with near oceanic salinities in the summer and late fall, to partially mixed in the winter and spring, and resembling a salt wedge during large discharge events. The Coos Estuary displays many features that complicate classic estuarine theory: strong tidal forcing, a short estuary (i.e. the length of tidal

excursion is comparable of length of salt intrusion; Ralston et al., 2010), channel curvature (Nidzieko et al., 2009), large bathymetric variability, fluctuating oceanic boundary conditions (Banas et al., 2004), and multiple tributaries with episodic freshwater input. For example, Roegner et al. (2001) measured periods when water entering South Slough from the main channel was fresher than the water in the slough (i.e. a reverse salinity gradient), and recent hydrographic observations show a more drastic example of the same process occurring in Isthmus Slough. To understand the dynamics, salt fluxes, and exchange flow, we develop a high resolution numerical ocean model of the Coos Estuary. The model is quantitatively evaluated using observational data from the estuary, and is then used to describe the dynamics and exchange flow throughout a seasonal cycle.

CHAPTER III

METHODS

Numerical Ocean Model

The Finite Volume Coastal Ocean Model (FVCOM, version 3.2.1) (Chen et al., 2012) is used to simulate flow and water properties in the Coos Estuary. FVCOM uses a finite volume discretization of the three dimensional, hydrostatic, primitive equations, and is well-suited for simulating coastal and estuarine environments with complex geometries. The finite volume formulation intrinsically ensures mass and salt conservation in the domain. FVCOM has been shown to be accurate to second order for barotropic test cases (Huang et al. 2008), and performs comparably to higher order schemes discretized on lower resolution, rectangular grids. An unstructured grid allows representation of complex geometries and variable horizontal resolution, here typically 15 m within the estuary (Fig. 1b), telescoping to 3 km at open boundaries. The grid inside of the estuary concentrates resolution inside of the deeper regions of channels, and the full domain extends over the continental shelf. The domain includes the mouths of the Umpqua River and Coquille River, although no freshwater is input from these sources. A sponge layer is applied at the oceanic boundary to reduce the impacts of the open boundary on estuarine dynamics. The domain inside of the estuary consists of multiple channels which extend either to end of the channel or beyond the length of tidal propagation. FVCOM allows wetting/drying of grid cells in intertidal areas, which compose a significant portion of the estuary. Vertically, twenty sigma layers are used. The grid used here has 195,000 triangular elements and 103,000 nodal points. To close the momentum equations, FVCOM employs the k-ε closure scheme from the General Ocean Turbulence model (Umlauf and

Burchard, 2003). Previous studies have used FVCOM to study estuaries with characteristics similar to the Coos, e.g. Yaquina Bay (Lemagie and Lerczak, 2015), on shallow tidal flats in the Skagit River (Ralston et al., 2013), and exchange flow and salt fluxes in the Merrimack River Estuary (Ralston et al., 2010, Chen et al., 2012).

Bathymetry

Bathymetry in the model domain is mainly sourced from a high resolution water-penetrating airborne LiDAR gridded at 1 m spacing (`https://coast.noaa.gov/htdata/lidar1_z/geoid12b/data/4905/or2014_usace_nwp_coosbay_m4905_metadata.html`) complemented by single beam sonar collected from a Coastal Profiling System (see Ruggiero et al., 2007) and channel surveys conducted by the U.S. Army Corps of Engineers (`http://www.nwp.usace.army.mil/Missions/Navigation/Surveys/`). Bathymetry data was weight-interpolated using MB-system (Caress et al., 2017) and then interpolated onto the model grid. For areas of the estuary where limited bathymetry data exist such as in the upper reaches of smaller channels, a linear along channel slope with uniform across channel depth was prescribed. Bathymetry on the model grid was smoothed to a limited degree in order to maintain the sharp bathymetry gradients that exist in this estuary due to recurring dredging. The bottom roughness length scale (z_0) was semi-empirically adjusted to a spatially constant value of 0.002 m. In numerical ocean models, this value represents a combination of roughness from skin friction as well as unresolved roughness due to bed forms and other factors. Many authors have noted the importance of z_0 for barotropic dynamics (Warner et. al, 2005, Wang et al 2009), and although the constant value used here generally has good skill (Table 1), in a future study this value should be more constrained, such as following Ralston et

al., (2017). Large bed forms (1 m) occur in the northern portion of the mouth of the estuary, and smaller bed forms are found in the natural, shallower tributaries of the estuary. Due to annual maintenance dredging in the main channel, the bed evolution in the main channel is unclear.

Boundary Conditions

Boundary conditions include river discharge at fourteen locations within the estuary (Fig. 1) and tidal forcing at the open boundary. Most freshwater enters the estuary through the Coos River (composed of S. Fork Coos River, W. Fork Millicoma River, E. Fork Millicoma River, and Marlow Creek), which is split into two inputs in the model domain. Multiple smaller creeks also drain into the estuary. Freshwater discharge data from the Coos Watershed Association (`http://www.cooswatershed.org/downloaddata/`) is used for the Coos River, while the remaining freshwater inputs are not measured, and are estimated based on watershed area. The estimated discharge magnitudes at Winchester Creek compare well with data collected prior to the time under investigation.

The model is forced at the boundary with elevations from the TXPO Tidal Model Driver (Egbert and Erofeeva, 2002), using 13 tidal constituents. Subtidal water levels from the Charleston tide gauge (NOAA station 9432780) were added to the TXPO water elevations to incorporate subtidal and tidal forcing. Salinity boundary conditions are enforced using reanalysis from a regional ocean model of the PNW (Giddings et al., 2014) that includes freshwater input from the Columbia River and upwelling and downwelling processes. The regional model mimics the seasonal cycle in salinity observed near the mouth of the estuary, as well as a Columbia River Plume intrusion event in July of 2014 that is also recorded in the

observations. However, discharge from other PNW rivers, and subsequently coastal buoyant currents (Mazzini et al., 2014), is not included in the boundary conditions.

Temperature is not included in the equation of state, because salinity dominates the density structure in the estuary. Local wind is neglected, as its effects are estimated to be secondary relative to the strong tidal forcing and river discharge. The model was initiated prior to the first discharge event of water year 2014 to obtain the correct salinity structure of the estuary, and the calendar year of 2014 is the focus of this analysis.

Observational Data

We use observational data from 2014 to describe the hydrography of the estuary and to validate the numerical ocean model. In-situ time series data was collected at multiple locations in the estuary in addition to monthly along-estuary hydrographic transects. The Charleston tide gauge (NOAA station 9432780) and water quality sensors (YSI model 6600) maintained by the South Slough National Estuarine Research Reserve (SSNERR) provide water elevations and salinity time series. SSNERR maintains sensors in Charleston (station 2, Fig. 1), Valino Island (station 3), Winchester Creek (station 4), Elliot Creek (station 5), as well as stations periodically maintained in the upper estuary: North Point (station 9), Isthmus Slough (station 11), Catching Slough (station 12), and in the Coos River (station 13). Two additional water quality sensors are maintained by the Confederated Tribes of the Coos, Lower Umpqua, and Siuslaw (CTCLUSI) water quality monitoring program, located at the Empire Docks (station 6) and Bureau of Land Management boat ramp (station 8). The sensors record data at 15 minute intervals; most stations have data gaps, and for some salinity records, an obvious drift towards lower salinities occurred. These erroneous data were removed from

the analysis. Monthly along channel Conductivity Temperature Depth (CTD) profiles were collected from 2012-2014, as described in Sutherland and O'Neill (2016). Twenty-five total along channel transects were taken during this time-period, and all but two were during flood tide. An upward looking Sontek 150 kHz Acoustic Doppler Current Profiler (ADCP) was deployed in the estuary from fall 2013 to July 2014, located on the channel flank (10 m depth) near the Empire Docks (station 7).

Total Exchange Flow

The isohaline, quasi-Lagrangian Total Exchange Flow (TEF) (MacCready, 2011) method is used to quantify the exchange flow in the estuary, as salinity dominates the density structure. TEF has the advantage of incorporating subtidal and tidal fluxes of volume and salt, and exactly satisfying the time dependent Knudsen relations (Burchard et al., 2018). Volume transport is classified as a function of a specific salinity class through a cross section, which contains transport due to both tidal and subtidal (e.g. river discharge, Stokes drift, gravitational circulation) processes. By using an isohaline framework, TEF elucidates areas of diapycnal mixing and the temporal variability of the full exchange flow. However, spatial information of the exchange flow cross sectionally is lost (i.e. from an Eulerian description), and there are currently no predictive forms of the TEF equations. TEF has been used to study exchange flow in the geometrically complex Salish Sea (Sutherland et al., 2011), as well as in estuaries where the Eulerian flow description does not encompass the total exchange flow: Merrimack River Estuary (Chen et al., 2012), Galveston Bay (Rayson et al., 2017), and the Columbia River Estuary (MacCready, 2011).

Following MacCready (2011), the isohaline transport function is defined as

$$Q(s) = \langle \int_{As} u dA \rangle, \tag{3.1}$$

where As is the area of a cross sectional element that has salinity greater than s, u is the velocity normal to the cross section, dA is the area of the cross sectional element, and the brackets indicate an average over the tidal cycle. In this study, all tidal averaging was done with a successive 24-24-25 hour Godin filter. Formally, to find the transport in a specific salinity class δs, Q is differentiated as

$$\frac{-\partial Q}{ds} = \lim_{\delta s \to 0} \frac{Q(s + 0.5\delta s) - Q(s - 0.5\delta s)}{\delta s}. \tag{3.2}$$

In practice, we can discretely bin salinity and volume fluxes through multiple cross sections in the estuary to obtain $\frac{-\partial Q}{\partial s}$, here using 1000 salinity bins over the range of salinity found in the estuary. MacCready et al. (2018) discusses two methods of integrating $\frac{-\partial Q}{\partial s}$ to find the inflowing and outflowing transports: one can integrate the inflowing and outflowing salinities based on the sign of transport within a salinity class

$$Q_{in} = \int \frac{-\partial Q}{\partial s}|_{in} ds, Q_{out} = \int \frac{-\partial Q}{\partial s}|_{out} ds, \tag{3.3}$$

where in/out refers to the direction of the volume flux through the cross section. The second method uses the global maxima of the integrated function Q(s) to find the inflowing and outflowing components. This method is more robust, as TEF transports converge for varying numbers of salinity bins (MacCready et al., 2018), whereas in the original method, changing the number of salinity bins varies calculated transports due to changes in sign of transport being aliased into the total values. Therefore, the second method is used in this study.

The inward and outward fluxes of salt through a cross section are defined as

$$F_{in} = \int s(\frac{-\partial Q}{\partial s}|_{in})ds, F_{out} = \int s(\frac{-\partial Q}{\partial s}|_{out})ds, \tag{3.4}$$

and the normalized salinities of the inflowing and outflowing layers are

$$s_{in} = \frac{F_{in}}{Q_{in}}, s_{out} = \frac{F_{out}}{Q_{out}}. \tag{3.5}$$

The TEF terms satisfy conservation of volume ($Q_{in} + Q_r + \frac{d\int dV}{dt} = Q_{out}$) and conservation of salt ($\frac{d\int sdV}{dt} = Q_{in}s_{in} + Q_{out}s_{out}$); which can be manipulated into a diagnostic solution for the inflowing volume flux:

$$Q_{in} = \frac{s_{out}}{\Delta s}Q_r + \frac{1}{\Delta s}\frac{d}{dt}\int sdV - \frac{1}{\Delta s}\frac{dV}{dt}. \tag{3.6}$$

Similarly to the classical salt flux decomposition method (e.g. Lerczak et al., 2006), fluxes through a cross section are also decomposed into a subtidal, spatially varying component, here denoted as the Eulerian component, and the remainder, which is due to tidal timescale correlations. The Eulerian values therefore represent the magnitude of the exchange flow which would be driven by the subtidal momentum balance. While similar to the classic salt flux decomposition, TEF differs in that tidal timescale correlations can contribute to the exchange flow, rather than parameterized as a diffusive process. The Eulerian component is found similarly to the total quantities, but tidally filtered velocity (and area elements) are binned according to tidally filtered salinity. The volume transports are decomposed into the Eulerian and tidal components as:

$$Q_{Eul}(s) = \int \langle u \rangle \langle dA \rangle \tag{3.7}$$

$$Q_T(s) = Q(s) - Q_{Eul}(s). \tag{3.8}$$

CHAPTER IV

MODEL EVALUATION

Model fields were output at hourly intervals, and observational data were interpolated onto the model times for comparison. To assess model skill, a linear correlation coefficient and model skill score were calculated. The correlation coefficient, r, measures the linear relationship between the observed (o) and modeled (m) values of a variable (x), where a value of r=1 indicates an exact linear relationship:

$$r = \frac{1}{\sigma_o \sigma_m N} \sum_{i=1}^{N} (x_m - \overline{x_m})(x_o - \overline{x_o}) \tag{4.1}$$

where σ is the standard deviation, and an overbar represents the mean. Model skill score (SS) is defined as the mean square error between the model and observations (Murphy, 1988), normalized by the squared standard deviation of observations:

$$SS = 1 - \frac{1}{\sigma_o^2 N} \sum_{i=1}^{N} (x_o - x_m)^2 \tag{4.2}$$

SS=1 when the model exactly replicates observations, SS=0 when the mean square error is equivalent to the standard deviation of observations (i.e. model has skill equal to the mean of observations), and SS is negative when the model is less predictive than the mean of observations. The skill score can also be represented as $SS = r^2 - (r - -\frac{\sigma_m}{\sigma_o})^2 - (\frac{\overline{x_m} - \overline{x_o}}{\sigma_o})^2$, where the middle term on the right side of the equation represents the normalized variance bias between the model and observations, and the last term on the right side of the equation represents the normalized mean bias (MB) between the model and observations. MB is calculated for salinity time series comparisons (Table 1), because for multiple stations MB causes a larger reduction in SS than the variance bias (e.g., the model is too fresh, but is simulating the variance properly).

Table 1. Model Skill Metrics for each station in the estuary.

The location of stations are shown in Fig. 1. Model skill score (SS, equation 10), the linear correlation coefficient (r, equation 9) and the mean bias (MB) are shown for the instantaneous and subtidal time series.

	water level	salinity	subtidal salinity	depth averaged velocity
Station	r (SS)	r (SS) (MB)	r (SS) (MB)	r (SS)
1 Charleston (NOAA)	0.998 (0.997)	-	-	-
2 Charleston (SNERR)	0.998 (0.995)	0.900 (0.773) (0.027)	0.906 (0.766) (0.023)	-
3 Valino Island	0.995 (0.989)	0.883 (0.751) (0.017)	0.915 (0.800) (0.022)	-
4 Winchester Creek	0.973 (0.902)	0.552 (0.098) (0.334)	0.821(-0.285) (1.00)	-
5 Elliot Creek	0.985 (0.970)	0.793 (0.342) (0.312)	0.887 (0.199) (0.444)	-
6 Empire	-	0.855 (0.723) (0.030)	0.927 (0.706) (0.065)	-
7 ADCP location	-	-	-	0.853 (0.707)
8 BLM	0.993 (0.983)	0.920 (0.589) (0.133)	0.887 (0.436) (0.363)	-
9 NorthPoint	0.993 (0.986)	0.849 (0.110) (0.22)	0.934 (-0.208) (0.884)	-
10 Coquille	-	0.729 (-0.776) (1.15)	0.869 (-1.63) (2.028)	-
11 Isthmus Slough	0.987 (0.973)	0.784 (0.204) (0.012)	0.887 (0.190) (0.543)	-
12 Catching Slough	0.988 (0.970)	0.865 (0.608) (0.183)	0.952 (0.781) (0.135)	-
13 Coos River	0.987 (0.968)	0.865 (0.612) (0.138)	0.975 (0.714) (0.194)	-

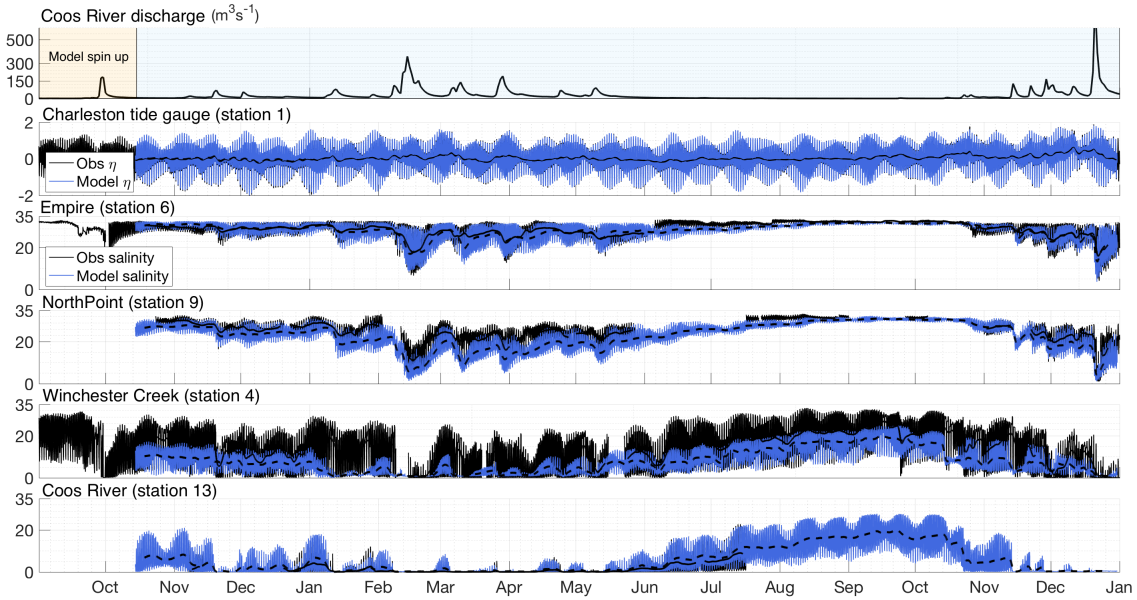

Figure 3. Model-data time series comparisons.
In all plots, the observations are colored black, modeled values blue, tidally filtered observations have a solid black line, and tidally filtered modeled values have a dashed black line. The top plot shows the time period of model spin up, and the discharge from the Coos River.

Water Elevations

The model has high linear correlation coefficients and skill scores for tidal elevation throughout the estuary (Table 1), with highest scores nearest the mouth of the estuary, and lower values in shallower tributaries. The lowest skill scores for water levels are in the upper reaches of South Slough at Winchester Creek and Elliot Creek. The amplitudes and phases of major tidal constituents, computed using T-TIDE (Pawlowicz et al., 2002), are shown in Table 2. The model matches the spatial patterns of tidal amplitude throughout the estuary, except in South Slough. In the main channel the total amplitude increases and reaches its maximum in Isthmus Slough in both observations and the model, while the total amplitude dampens relative to the main channel in both Catching Slough and the Coos River. The spatial patterns of total amplitudes in the model deviate from

observations in South Slough, as the observations show a decrease in amplitude landward (to Winchester Creek) and the model shows an increase in amplitude, although the amplitude in Elliot Creek is larger than Charleston in both the model and observations. The model reproduces tidal constituent amplitudes and phases well, as shown for the largest tidal constituents in Table 2. The subtidal water level at Charleston is exactly reproduced in the model (Fig. 3). The model captures the phasing of different constituents, and shows the difference in phasing between Isthmus Slough and the sensors up estuary from Marshfield channel.

Velocity

At the ADCP location, the modeled and observed velocity data were rotated 9 degrees to be oriented in the along channel direction, corresponding to the principal component direction as well. The ADCP was located on the flank of the main channel at 10 m depth, but captured velocity variability at tidal and subtidal timescales. At tidal timescales, the velocity is strongest during ebb tides, where surface currents vary from greater than 1.5 ms^{-1} during spring tides and 0.8 ms^{-1} during neap tides, as opposed to flood tides which rarely exceed $1ms^{-1}$. The model reproduces the tidal asymmetry in current strength (Fig. 4, Table 1) as well as the fortnightly modulation in magnitude. The subtidal (i.e. tidally filtered) along channel velocity from the model shows a two-layer structure that is temporally consistent with observations. Larger subtidal velocities occur during neap tides, when there is larger vertical shear and stratification, as well as after discharge events when the along estuary baroclinic pressure gradient strengthens. During spring tides isohalines straighten, the subtidal velocity decreases, and the direction of the subtidal velocity is predominately oceanward. As discussed in Section 3.5,

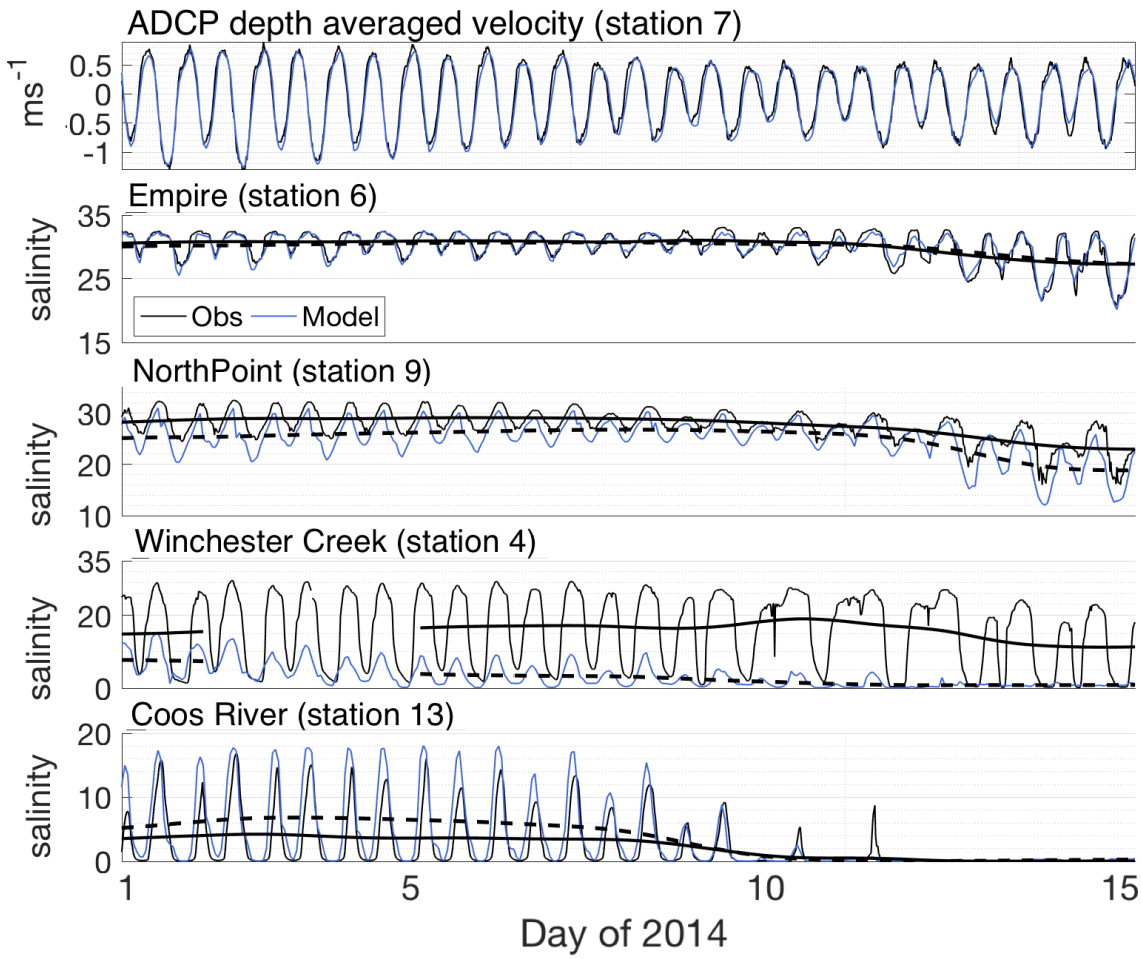

Figure 4. A zoom in of comparisons from Fig. 3 showing a 15 day period in January 2014
a) is a comparison between the depth averaged along channel velocity from the ADCP location (station 7), and the remainder of the plots are salinity time series comparisons at the same locations as Fig. 3.

Table 2. Tidal Comparisons between the model and observations.

The total amplitude and three largest tidal constituents are shown, extracted from T-Tide (Pawlowicz et al., 2002).

station	tidal amp. (m) obs, model	m2: amp.(ϕ) obs, model	s2: amp.(ϕ) obs, model	o1: amp.(ϕ) obs, model
Charleston (NOAA)	2.502, 2.521	0.817(198.2), 0.808(198.3)	0.202(275.8), 0.201(273.6)	0.009(53.8), 0.009(55.5)
Charleston (SNERR)	2.522, 2.537	0.811(199.7), 0.808(199.4)	0.202(277.5), 0.200(274.9)	0.009(59.3), 0.009(55.7)
Valino Island	2.492, 2.572	0.802(206.5), 0.812(202.9)	0.197(286.3), 0.200(279.7)	0.010(69.9), 0.010(62.5)
Winchester Creek	2.378, 2.627	0.695(209.3), 0.798(207.3)	0.154(290.8), 0.186(286.7)	0.013(87.7), 0.012(82.5)
Elliot Creek	2.596, 2.619	0.792(213.2), 0.775(205.1)	0.189(295.5), 0.204(286.9)	0.011(83.0), 0.014(83.4)
BLM	2.637, 2.670	0.852(207.9), 0.845(206.0)	0.205(287.9), 0.206(283.5)	0.009(56.3), 0.010(60.9)
NorthPoint	2.646, 2.677	0.870(311.8), 0.868(309.6)	0.210(343.5), 0.206(338.5)	0.217(310.8), 0.221(307.0)
Isthmus Slough	2.882, 2.869	0.903(38.3), 0.913(33.0)	0.220(108.4), 0.224(99.9)	0.196(156.2), 0.209(147.4)
Catching Slough	2.431, 2.444	0.912(347.9), 0.914(345.7)	0.264(137.3), 0.273(132.6)	0.191(318.6), 0.203(316.2)
Coos River	2.262, 2.426	0.886(246.0), 0.909(242.9)	0.177(261.6), 0.181(253.2)	0.151(41.1), 0.175(36.9)

the subtidal velocities are associated with the Eulerian component of the exchange flow.

Salinity

The numerical model simulates the complex spatial and temporal patterns of salinity variability within the estuary. Nearest the mouth of the estuary at Charleston, Empire and BLM stations, the model replicates salinity variability within the tidal cycle (Fig. 3). The tidal variability at these stations during the dry season is a few psu, while in the wet season is typically 5-10 psu, and as large as 20 psu during discharge events. At these stations, larger tidal variability in salinity is present during spring tides compared to neap tides due to advection length scales. In the main channel at North Point (16 km from the mouth), the tidal salinity variability is larger but similar patterns regarding spring-neap variability and response to discharge events remain. At this station and Coquille, the model has a mean fresh bias, as seen in the tidally filtered time series (Fig. 3,4), and the MB calculation in Table 1. The discrepancy may be due to a number of factors: over-estimated freshwater fluxes, unknown bathymetry in the upper reaches of channels. At shallow locations, small changes in freshwater flux can change the location of salinity fronts, such as in Winchester Creek, where the model does not capture the extreme tidal variability of salinity (e.g. 30 psu, Fig. 3), and the salinity front in the model is located a few hundred meters ocean-ward of the sensor. In Isthmus and Catching Slough the model generally represents the subtidal variability, but does not capture the full tidal variability as seen in the observations (i.e. changes of 5-10 psu within a tidal cycle). However, the model does well in simulating the salinity variability at the Coos River sensor, located 33 km from the mouth of the estuary; the model simulates the horizontal salinity gradient correctly, but

there are local discrepancies. The salinity increases at this location coinciding with spring tides and decreasing river discharge, and goes to fresh water during discharge events. The strong spring-neap variability seen at all locations highlights the dominance of tidal processes in this system. Tidally averaged salinities show better skill at all stations (Table 1), and follow the temporal patterns seen in the observations. During the dry season, the salinity boundary implementation does represent the full exchange between the coastal ocean and estuary, as the observations have higher salinities than the model (Fig. 3). This is somewhat expected, as there is no advective fluxes imposed at the boundaries or wind stress to initiate the upwelling of saltier water onto the continental shelf.

C.T.D. Profiles

Comparisons between CTD observations and the model show that the model is biased towards lower salinities (average 4 psu) and slightly lower vertical stratification (average 1 psu) than observations. One source of error in the comparisons is that model output is on hourly intervals, so that at maximum there is a thirty minute time lag between the two, which could result in an error of approximately 0-5 psu based on advection time scales. Along estuary plots of CTD comparisons of salinity in February and July (Fig. 5, 6) show that the model represents the spatial pattern along the estuary during the wet and dry season. The aforementioned biases can also be seen in the along estuary plots; a mean bias towards fresher salinities in July, and a reduced vertical stratification as compared to observations in February of 2014.

In summary, the numerical ocean model simulates the spatial and temporal dynamics of estuary, including high skill for tidal propagation (Table 1), moderate to good skill for salinity, and good skill for depth averaged velocity. The model has

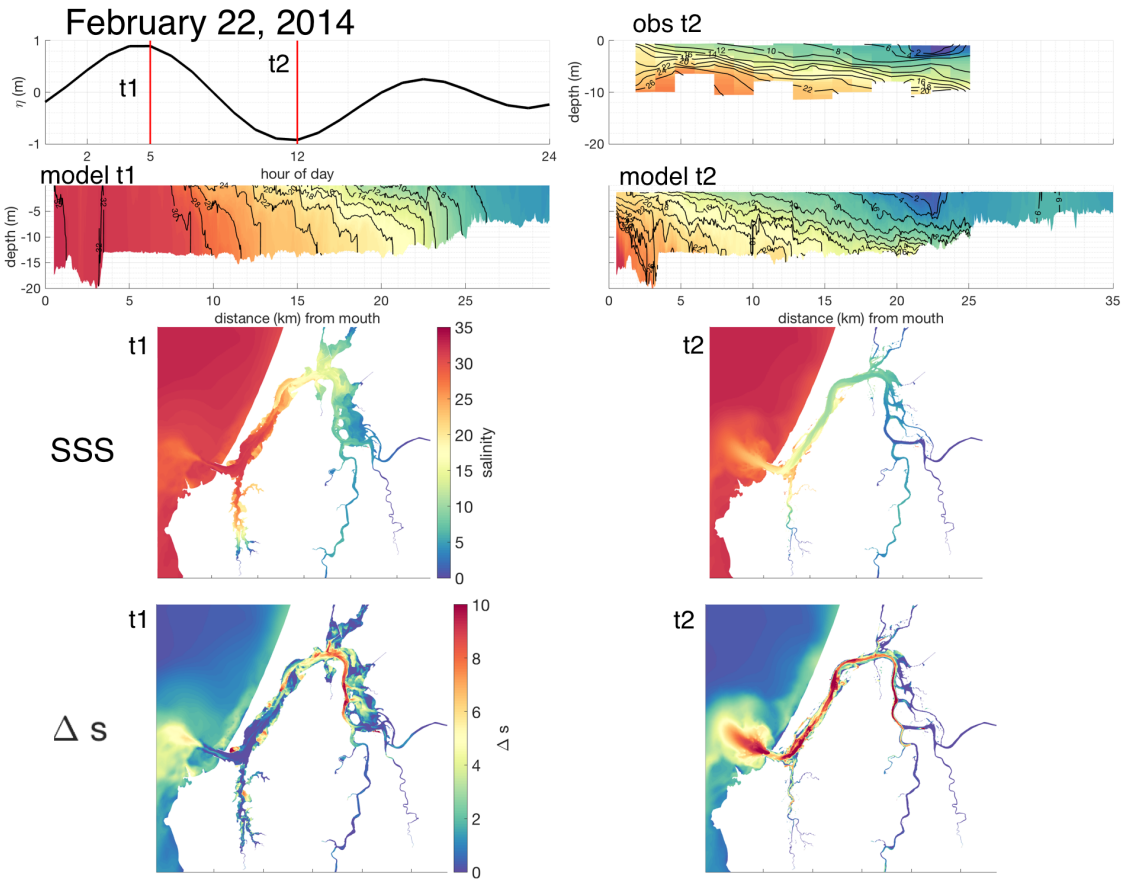

Figure 5. Comparison between the model and an along estuary CTD transect on February 22, 2014.
Comparisons are shown at the end of flood (t1) and end of ebb (t2), when CTD profiles were taken. Along estuary transects are shown, which go from the mouth of the estuary into Isthmus Slough. Sea surface salinity (SSS) is shown, and the top to bottom difference in salinity at t1 and t2.

a fresh bias in the main channel relative to observations for both CTD profiles and time series (Fig. 3). In some cases, the model does not capture the correct spatial location of horizontal salt gradients (e.g. Winchester Creek and Elliot Creek), or does not capture the tidal variability of salinity (e.g. Isthmus Slough and Catching Slough) but simulates the tidally averaged salinity, the response to discharge events, and the seasonal changes in salinity throughout the estuary properly. Improving model performance would entail using more accurate bathymetry for the upper

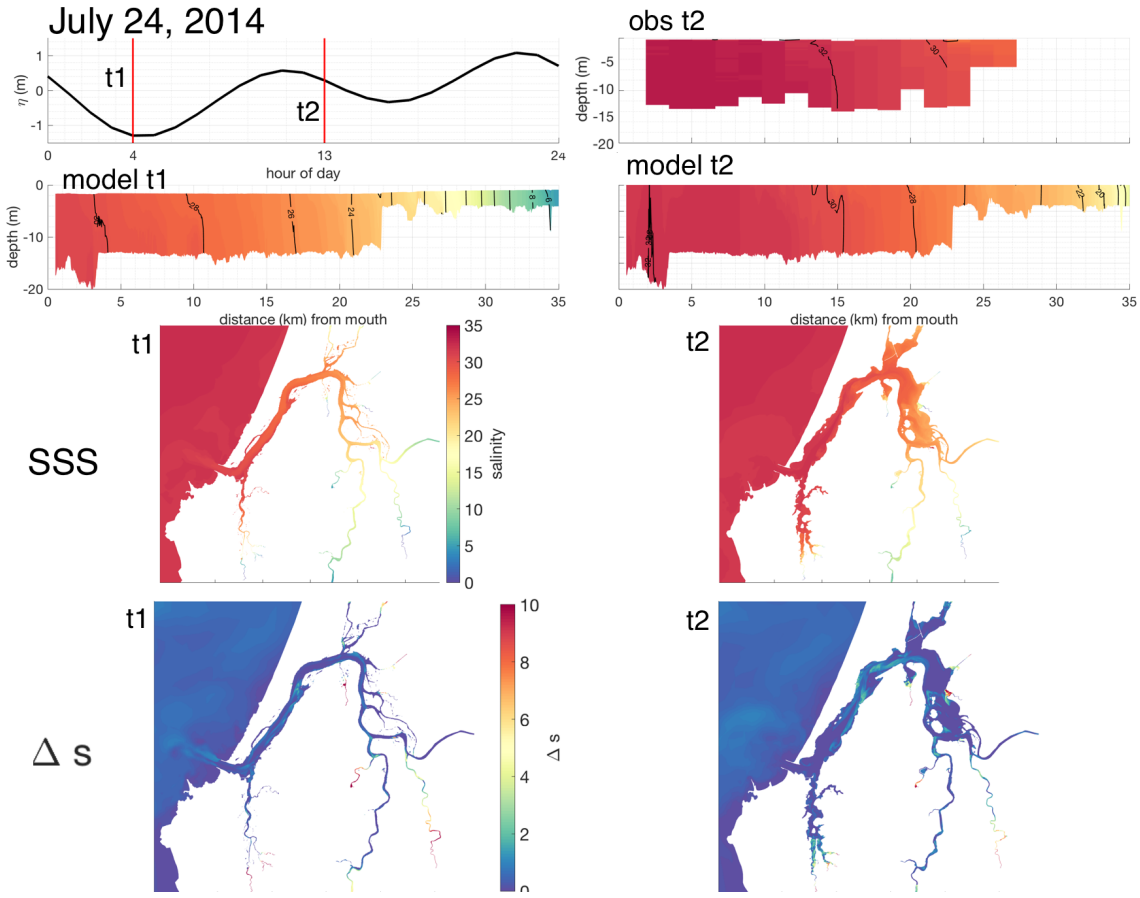

Figure 6. Comparison between the model and an along estuary CTD transect on July 24, 2014.
Comparisons are shown at the end of ebb (t1) and beginning of ebb (t2), when CTD profiles were taken. Along estuary transects are shown, which go from the mouth of the estuary into Marshfield Channel. Sea surface salinity (SSS) is shown, and the top to bottom difference in salinity at t1 and t2.

reaches of the estuary, and empirically obtaining better estimates for freshwater discharge from the smaller creeks into the estuary. The magnitudes of discharge, although small in comparison to the Coos River, are important for obtaining the correct spatial structure of the salinity field in the shallow channels. As for the mean bias in the main channel, it is unclear what is causing the discrepancy, as the estimated smaller creek discharges are not significant fraction of the total amount. It is possible that the horizontal resolution in the dredged, narrow main channel

is not adequate to simulate the total subtidal landward salt transport, and that the boundary conditions do not allow enough salt into the domain. Additionally, enhanced numerical diffusion of salinity gradients (Ralston et al., 2017) could limit the subtidal landward salt transport associated with the baroclinic pressure gradient.

CHAPTER V

RESULTS

Velocity and Salinity Structure

Tidal Dynamics. Velocity in the main channel is ebb-dominant (Fig. 4), caused by increased frictional dissipation over the tidal flats during flood tide (Blanton, 1969). The highest velocities occur near the mouth of the estuary (Fig. 7c) and in the dredged main channel, as well as in Marshfield Channel and other shallow regions of the estuary. The high ebb velocities are efficient in transporting mixed water out of the estuary every tidal cycle (Stommel and Farmer, 1952). Lateral shear in the along channel velocity produces lateral salinity gradients on both flood and ebb tide (Fig.7b); during ebb tide the main channel is fresher than the flanks, and during flood tide the main channel is denser than the flanks. During flood, differential advection of denser water in the center of the channel (Nunes and Simpson, 1985) drives lateral flows (Lerczak et al., 2004) creating a surface convergence zone in the center of the channel. Fig. 7c shows the divergence of surface velocity averaged over the year of 2014; averaging over the year smooths out tidal variability, but shows mid-channel convergences. At low water, a large portion of the estuary is dry (Fig. 5), including the East Bay tidal flats as well as all but the deeper narrow channels in tributaries, excluding the Coos River, where there are no intertidal areas.

During ebb tide the vertical stratification is greater due to the vertical shear in velocity and advection of the horizontal salinity gradient (Fig. 5) as the salinity field strains horizontally (Simpson et al., 1990). In South Slough and the Coos River/Marshfield channels, shallow depths lead to the formation of large horizontal and vertical salinity gradients. During strong ebbs, however, the velocity in these

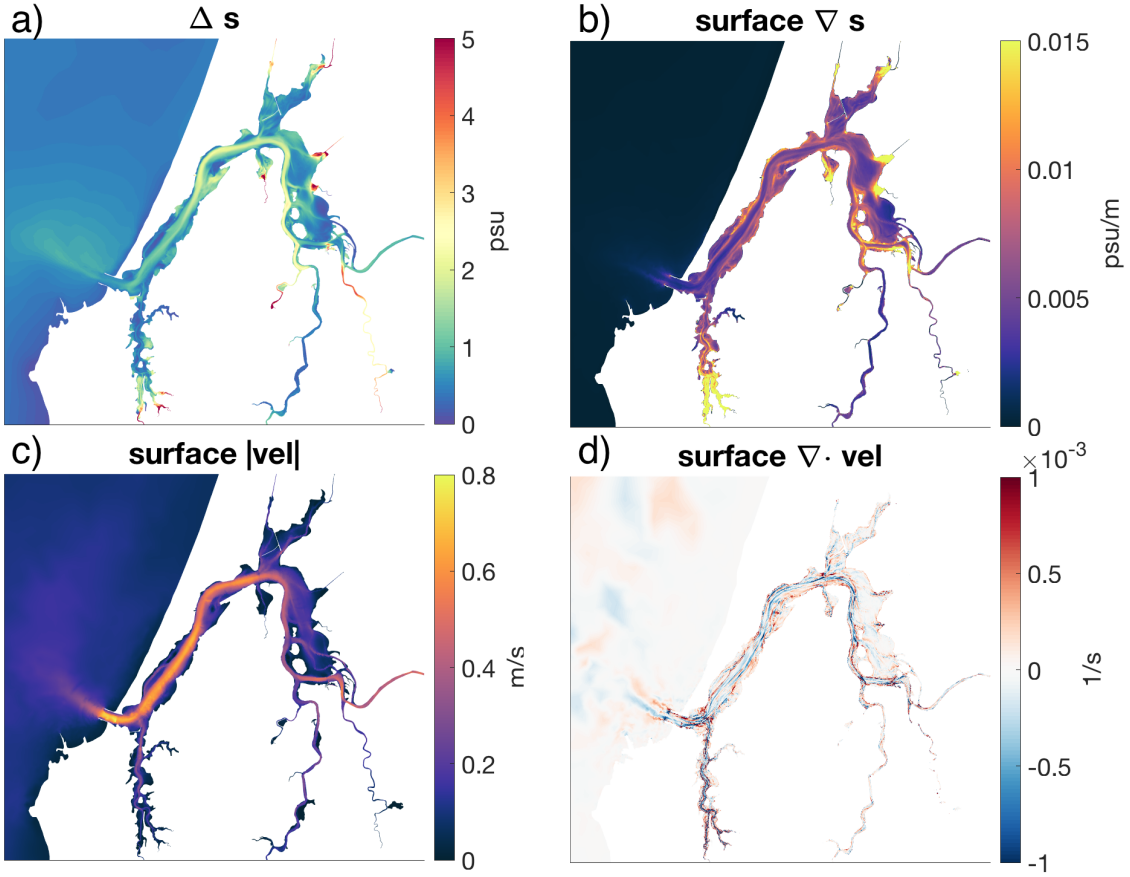

Figure 7. Spatial patterns of salinity and velocity averaged over the year of 2014. a) Top to bottom salinity stratification. b) The magnitude of the horizontal gradient of surface salinity. c) The magnitude of surface velocity. d) The divergence of surface velocity. Cool colors represent convergence while warm colors represent divergence.

shallower tributaries is strong enough that vertical shear overcomes the vertical stratification and the water column becomes vertically well mixed. During flood tide, vertical mixing of salt and momentum extends upward in the water column from the bottom boundary layer, which acts to vertically straighten isohalines. Water from the coastal ocean enters the estuary and is advected roughly 8-12 km up the estuary, both in the main channel and South Slough. At the end of flood, the barotropic pressure gradient changes directions and ebb currents over the East Bay tidal flats create a frontal convergence zone over a large portion of the eastern estuary (Fig. 5). Strong horizontal fronts are found throughout the estuary (Fig. 7b), due to the multiple freshwater inputs and the local differences in advection patterns throughout the estuary. The horizontal salinity gradients depicted in Fig. 7b show average frontal locations, but spatial locations are highly variable throughout the tidal cycle. Fronts represent strong local gradients in the horizontal salinity field, where flow convergences induce vertical velocities and tend to aggregate organisms and buoyant particulates (Largier, 1992).

Seasonal Variability. Seasonally, the hydrography of the estuary changes substantially (Fig. 5, 6; Sutherland and O'Neil, 2016), with the largest changes occurring in the main channel, as the difference between summer and winter Q_r in the Coos River is much greater than the difference in tributary creeks. Vertical stratification in the changes from greater than 10 psu in the winter during discharge events to 1-2 psu in the summer, although high vertical stratification is present in the summer near the heads of tributaries (Fig. 7a). The tidal variability of salinity at individual stations decreases as the dry season continues (Fig. 3) due to decreased horizontal salinity gradient. However, tidal velocities and tidal excursion length scales are similar year round, modulated by the sping-neap cycle.

The salt content of the estuary has pronounced tidal variability (Fig. 10c), which is of the same magnitude as the seasonal change in total salt in the estuary (tidally filtered in Fig. 10c).

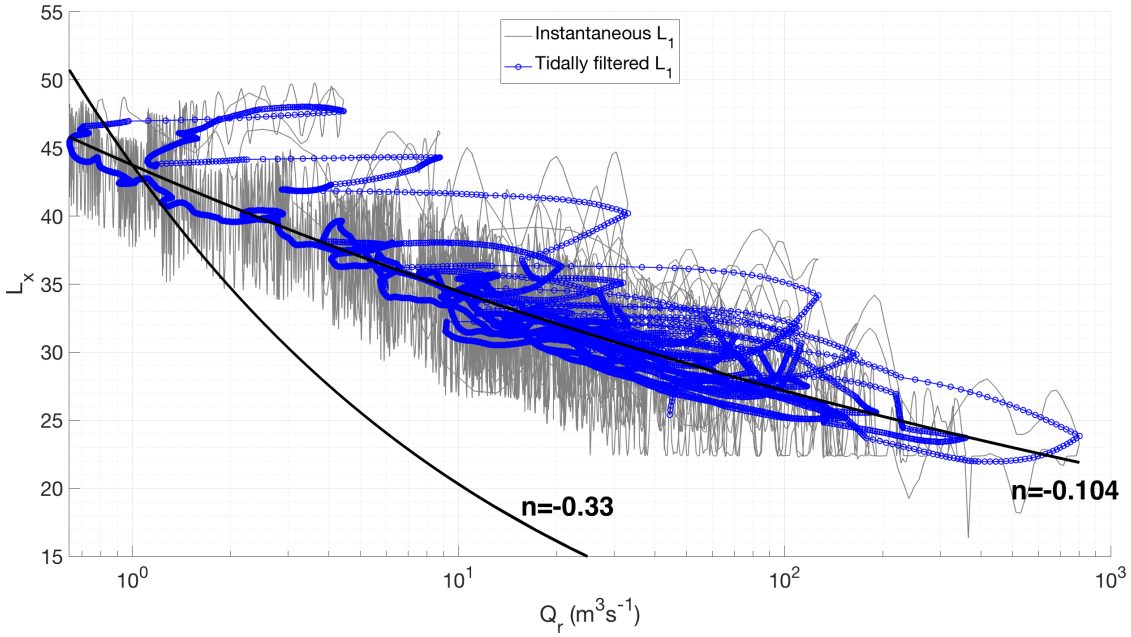

Figure 8. Relationship between river discharge and the length of the saline intrusion.
River discharge from the Coos River (x-axis), compared with the length of the salinity intrusion going from the main channel up Coos River for the year of 2014. The length of the salinity intrusion is defined as the extent to which the depth averaged salinity is less than 1 psu (L_1), shown instantaneously by the gray line and tidally filtered by the blue line. Power law relationships of the form $L_x - Q_r^n$ are shown in black.

The horizontal salinity gradient, represented by the length of the salt intrusion (Fig. 10c), decreases as Q_r diminishes in the dry season. Steady estuarine theory predicts the length of the salinity intrusion L_x is related to the river discharge as Q_r^n, where $n = -0.33$ (Hansen and Rattray, 1965; Monismith et al., 2002). Here, the length of the estuary is defined as the nearest oceanward location that has a depth averaged salinity less than one psu, going up the Coos River/Marshfield Channel from the mouth of the estuary. Using this definition,

the length of the estuary displays and even more muted response to discharge (Fig. 8) than other estuaries in the literature (e.g. n=-0.14, Monismith et al., 2002), and estimates from observations from the main channel by Sutherland and O'Neil (2016) (n=-0.19). This response is due to the bathymetry and geometry of the estuary; the lower limit of the length of the estuary corresponds to the junction of Marshfield channel and the main channel. The deep, dredged channel prohibits this definition of the estuary to move any further oceanward, as the discharge from the Coos River would have to be strong and persistent enough to fill up the main channel and Isthmus Slough with freshwater. Using the 15 psu isohaline instead of 1 psu increases the coefficient to n=-0.14, more in line with the fit from observations (Sutherland and O'Neil, 2016). The length of the estuary varies roughly 10 km over the tidal cycle (grey line in Fig. 8), but no discernible changes in L_1 are found that correspond to changes in the spring-neap cycle.

Total Exchange Flow

To quantify the estuarine exchange flow, the TEF method is applied to the estuary throughout the year of 2014. Investigation of the isohaline transport in the upper estuary revealed a complex expression of water mass transport, as noise in $\frac{-\partial Q}{\partial s}$ is substantial up estuary from one tidal excursion from the mouth, resulting in a non-smooth Q(s) during various times of the year. This can be seen in Fig. 9, where $\frac{-\partial Q(x,s)}{\partial s}$ and Q(x,s) (x denotes spatial location along estuary) is compared at multiple cross sections along the estuary at two snapshots in time. $\frac{-\partial Q(x,s)}{\partial s}$ coherently shows two classes of inflowing and outflowing salinities near the mouth, while $\frac{-\partial Q(x,s)}{\partial s}$ at up estuary cross sections shows many sign changes, which can result in a non-smooth Q(x,s).

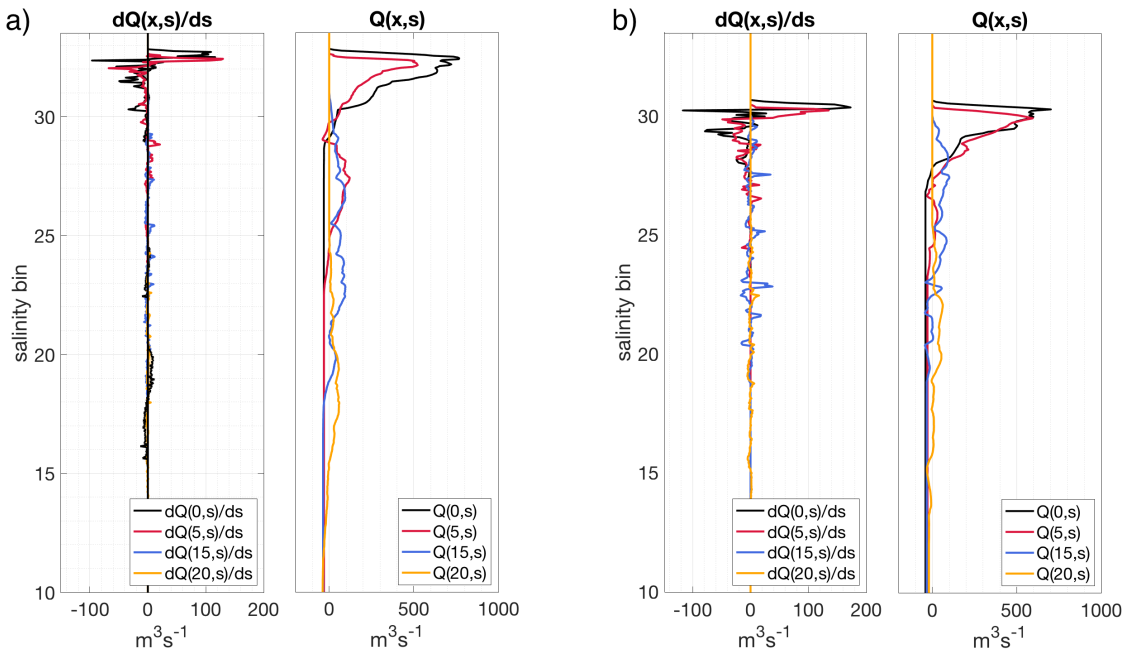

Figure 9. Snapshots of TEF transports throughout the estuary. $\frac{-\partial Q(x,s)}{\partial s}$ and Q(x,s) are shown for cross sections located at 0, 5, 15, and 20 km from the mouth of the estuary. Positive volume fluxes (x-axis) are directed into the estuary. a) shows a snapshot on March 5, 2014, while b) is on July 15, 2014.

The reason for the variability in Q(s) is unclear, but it is speculated that the advection of varying salinity classes throughout a cross section over the mixed semi-diurnal tidal cycle and mixing of various salinity classes during the tidal cycle results in the transport seen in $\frac{-\partial Q}{\partial s}$. It was hypothesized that this variability was due to different portions of a cross section transporting separate water masses, but $\frac{-\partial Q}{\partial s}$ from a cross section in just the main channel was similarly as noisy as the full cross section. Q(s) becomes less coherent during spring tides, and is smoother during river discharge events and neap tides, indicating that the transport that causes the large variability in Q(s) is due to the large tidal fluxes. Note that the Eulerian version of isohaline transport ($\frac{-\partial Q_{Eul}}{\partial s}$) shows a coherent structure of subtidal water mass transport as compared with $\frac{-\partial Q}{\partial s}$. How the variability in Q(s)

influences the TEF calculations is unclear, but, similar temporal patterns in the TEF variables from near the mouth of the estuary, where Q(s) is smooth and in the upper estuary where Q(S) is non-smooth, suggests that TEF is capturing the exchange flow in the estuary. One solution would be to integrate transport based on local minima and maxima of Q(s), which would result in multiple layers of exchange flow. However, to separate the transport in the main channel into multiple layers would only complicate the interpretation of the exchange flow, and is not done here.

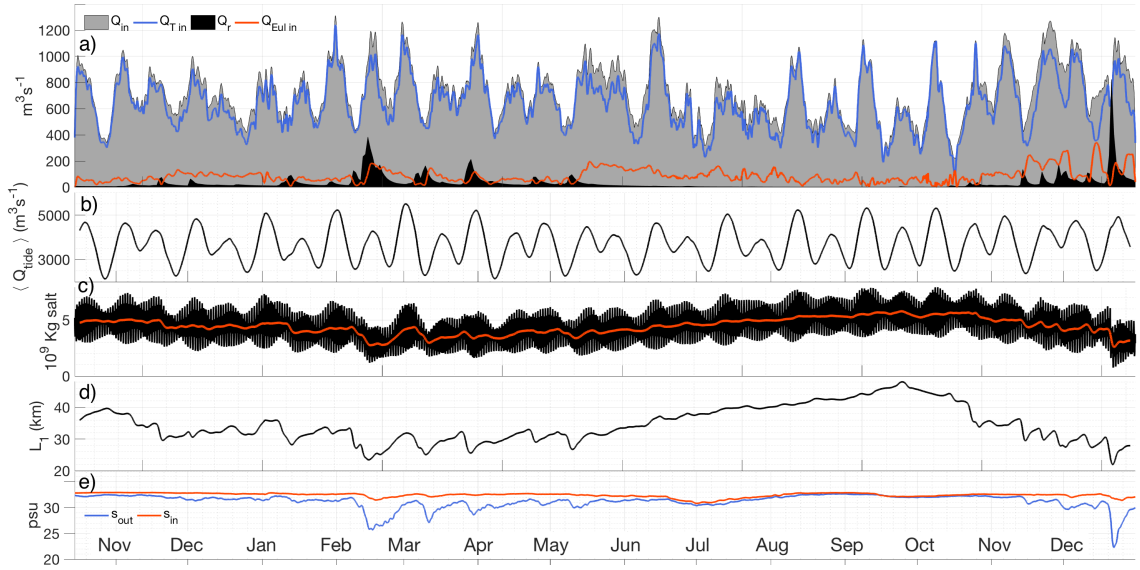

Figure 10. Estuarine variability throughout the year of 2014.
a) Fluxes (m^3s^{-1}) at the mouth of the estuary. b) Q_{tide} (equation 12). c) Total salt content (10^9 Kg) in the estuary. d) Length of the estuary, defined using the depth averaged 1 psu isohaline going up the Coos River. e) Inflowing and outflowing volume weighted salinities at the mouth of the estuary.

Exchange Flow Variability. The inflowing component of the exchange flow at the mouth of the estuary varies between 300-1200 m^3s^{-1} over the year of 2014 (Fig. 10a); therefore amplified over the river flow by roughly one to three orders of magnitude, the latter occurring during the summer when discharge is low and the exchange at the mouth is still vigorous. Q_{in} varies smoothly along the

estuary, and the temporal variability of Q_{in} relative to the mean is near constant along the estuary. However, Q_{in} sharply decreases beyond one tidal excursion of the mouth (Fig. 11a). The dominant variability of the exchange flow, as seen in the phasing of Q_{in} (Fig. 11a), is associated with the fortnightly spring-neap cycle, being greater during spring tides and reduced during neap tides through out the estuary. This is contrary to the classical expectation for partially mixed estuaries (Geyer, 2000; Lerczak et al., 2006) and the theory of gravitational circulation; during neap tides, reduced vertical mixing increases vertical stratification and velocity shear, which acts to increase the exchange flow and upstream salt flux. During spring tides, even though horizontal advection length scales are larger, the greater tidal velocities result in increased turbulent mixing, which decreases vertical stratification and shear, and inhibits the upstream flux of salt. However, the time variability is consistent with recent studies documenting exchange in short estuaries with strong tidal forcing (Ralston et al., 2010; Chen et al., 2012), as well as many estuaries classified using the Eulerian salt flux decomposition (e.g. Lerczak et al., 2006), where the tidal component of the total salt flux was the main contributor. The TEF framework is able to capture the persistent exchange flow, while the Eulerian component is a small and spatially variable component of the full exchange flow.

The tidal component is the main contributor of exchange flow in the estuary (grey colors in Fig. 11b), but the Eulerian component is persistently enhanced at specific cross sections. A similar along channel variability in the partitioning was also found in the Hudson River Estuary (Chen et al, 2012; Wang et al., 2015), where Q_{in}^{Eul} can be greater than Q_{in}, such that Q_{in}^{T} acts in a up gradient direction. Along channel variability in the Eulerian version of exchange flow would imply

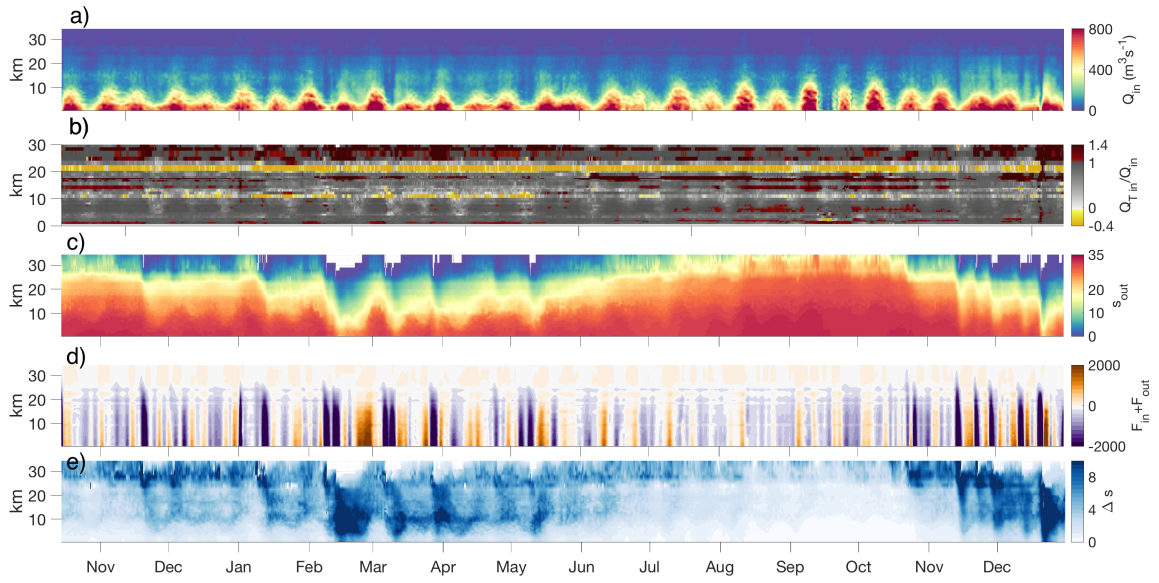

Figure 11. Along estuary exchange flow variability throughout the year of 2014. In all plots, the x-axis is the month of 2014 and the y-axis is distance up estuary (km) from the mouth up Marshfield Channel and the Coos River. a) $Q_{in}(m^3s^{-1})$. b) the fraction of Q_{in} that is represented by Q_T (equation 8). Note that negative values mean $Q_{Eul} > Q_{in}$. c) s_{out}. d) $F_{in} + F_{out}$ (note that F_{out} is defined as negative, so that a positive value of the summation represents a gain of salt). e) $\Delta s = s_{out} - s_{in}$.

local convergences in the subtidal flow; however, the TEF volume fluxes are smooth throughout along the estuary, such that the tidal component exactly compensates for the along channel variability in Q_{in}^{Eul} (Wang et al., 2015). In the Coos Estuary, there are three locations where the Eulerian term is relatively large (yellow colors in Fig. 11b), which correspond to along channel changes in cross sectional geometry. Near 3 km from the mouth the depth transitions from 20 m to 14 m (Fig. 2a), and at 10.5 and 20.5 km from the mouth, where the channel widens (Fig. 1, Fig. 2b) and Q_{in}^{Eul} is largest (Fig. 11b). During tidal timescales, vertical fluctuations in the position of the halocline result in a distortion of the subtidal Eulerian flow field, which can be manifested as increased tidal component of exchange (Geyer and Nepf, 1996) or a counter-gradient tidal flux, as in these cross sections. At these

three cross sections, it appears that during ebb tide, supercritical flow develops in the regions where cross sectional areas abruptly increase (Geyer et al., 2017), leading to an elevated halocline during ebb tide (Wang et al., 2015). This causes a tidal asymmetry in fluxes of volume and salt result in enhanced Q_{in}^{Eul}. Conversely, at some locations in the estuary, the tidal component of the exchange flow is greater than that total (red colors in Fig. 11b).

The Eulerian component of the exchange flow is dependent on river discharge and the seasonality of the horizontal salinity gradient, increasing during the wet season when the horizontal salinity gradient is stronger. The Eulerian component is also dependent on the strength of tidal mixing, as it increases during neap tides, and in general increases as going up the estuary. Upon leaving the main channel and going landward up Marshfield Channel and the Coos River, the tidal component again dominates, consistent with a shallower regime (4m) and strong horizontal and vertical salinity gradients. The estuary responds rapidly to discharge events, as seen in the normalized salinity of the outflowing layer (Fig. 11c), and the net gain and loss of salt (Fig. 11d). Salt is expelled from the estuary during discharge events and rapidly gains salt after the freshwater flux into the estuary has subsided. However, the fluxes of salt throughout the estuary are in phase with Q_{in} and Q_{out} (eqn. 4). During spring tides, the estuary also tends to gain salt, while loosing salt during neap tides. The TEF stratification, Δs is shown for the year throughout the estuary in Fig. 11e. During the winter, the TEF stratification reaches background values of 3-4 psu, and during discharge events can be 7-10 psu. The dominant control on Δs is by the river discharge, but Δ slightly increases during neap tides as well. In the main channel, the stratification subsides in the dry season, but persists in the shallower Marshfield Channel and Coos River channels.

Dynamics of Tributaries

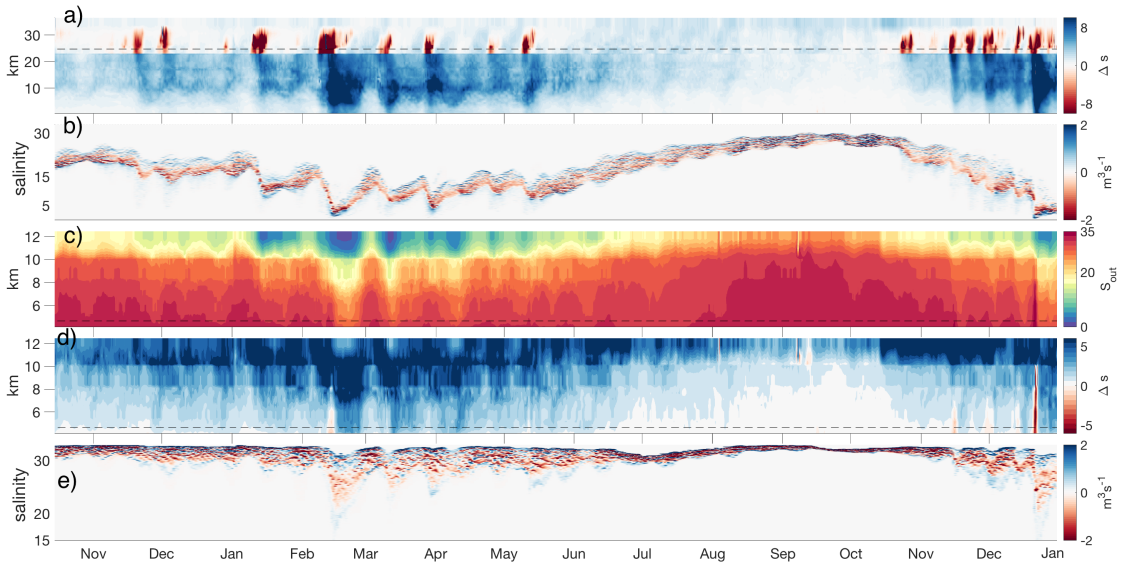

Figure 12. Variability of exchange flow in the Tributaries of the estuary. a) Δs, for the year of 2014 (x-axis), from the mouth of the estuary up Isthmus Slough (y-axis, in km); $-\Delta s$ means that the inflowing layer is fresher than the outflowing layer. The dashed line represents the location of the cross section used in b), showing $\frac{-\partial Q}{\partial s}$. c)-e) show TEF variables for the year in South Slough, where the y-axis is distance (km) from the mouth. c) S_{out}, d) Δs; the dashed line shows the location of the cross section used in e), showing $\frac{-\partial Q}{\partial s}$.

The geometry and bathymetry of the estuary dictates the velocity structure and the transport of freshwater and salt throughout the estuary, affecting tidal dispersion throughout the estuary, and creating regions of reversed horizontal salinity gradients. In many tributaries, the velocity and salt transport is not in phase with the main channel, as the shallower tributaries respond quicker to changes in the barotropic pressure gradient than the deeper main channel (MacVean and Stacy, 2011). In the upper estuary, the currents begin to ebb in Catching Slough prior to the Coos River. Freshwater from the Coos River and Catching Slough is then partitioned between Marshfield channel and the East Bay tidal flats. Near the end of ebb, freshwater from Marshfield Channel enters

the main channel, upon which flood begins and the freshwater is subsequently transported up Isthmus Slough. A similar process was documented in San Francisco Bay (Warner et al., 2001; MacVean and Stacey, 2011), where the along channel reversal in the baroclinic pressure gradient created a convergence zone in the subtidal velocity field.

Pulsing of freshwater into Isthmus Slough creates a reversal of the local along estuary salinity gradient, coinciding with an abrupt sign change in Δs associated with passing the junction between Marshfield Channel and the main channel (Fig. 12a). In the TEF framework, changes in sign in Δs represent a reversal of exchange flow with respect to the salinity coordinates. Negative Δs therefore represents periods when the inflowing water is on average fresher than the outflowing water. The full variability of subtidal volume transport within salinity classes is shown in $\frac{-\partial Q}{\partial s}$ (Fig. 12b). The reverse circulation persists on similar time scales as the discharge events, and eventually, once the fresher water has mixed, the sign of Δs switches back to normal. During the reversals, a subtidal flow convergence of bottom waters occurs at the transition of the sign change in Δs. Bottom flow convergence has important implications on sediment transport and the formation of estuarine turbidity maxima. Similarly, Roegner and Shanks (2001) documented fresher water from the main channel intruding into South Slough. In the TEF framework, fresher water commonly enters South Slough (Fig. 12e) from the main channel, and reversals in Δs are seen during the largest discharge events. It is also hypothesized that phase offsets in velocity between the main channel and adjacent channels could result in a retardation of the flow in the main channel, therefore having an impact on residual circulation patterns and transport in the main channel, but this is not investigated.

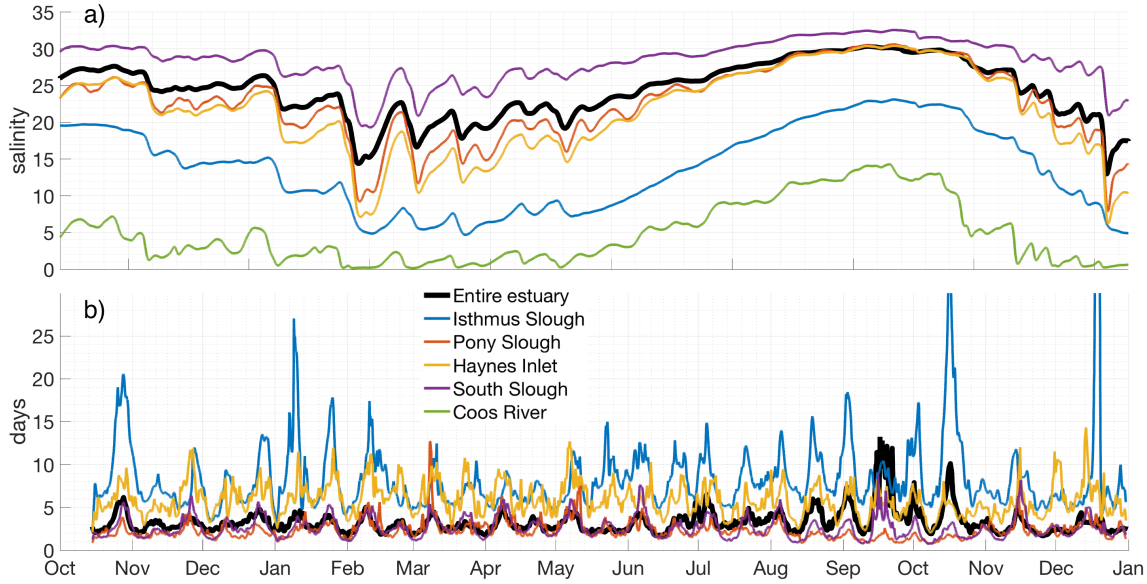

Figure 13. Residence time variability.
a) Mean salinity for each basin. b) T_{res} in days for each basin.

Residence Time. TEF volume fluxes can readily be applied to the tributaries in the estuary to estimate the temporal variability of residence time. Water residence time is defined as

$$T_{res} = \frac{\langle \int dV \rangle}{Q_{out}}, \tag{5.1}$$

and is shown for the main estuary and smaller channels in Fig. 13. The saltier channels of the estuary generally have lower residence times as they are closest to the ocean. The longest residence times are found in tributaries in the upper estuary (Isthmus Slough and Haynes Inlet), where the longest values are around 15 days. The periodicity of T_{res} inversely follows Q_{in}, such that longer residence times occur during neap tides. These times should be taken as a rough estimate, as T_{res} is only fully accurate if complete mixing of the estuarine volume occurs over a timescale much shorter than T_{res} itself. Lemagie and Lerczak (2015) showed that the estuary integrated T_{res} significantly underestimated flushing times in Yaquina Bay during

low river flow periods in the riverine portion of the estuary as compared with lagrangian particle tracking, while similar results between the two methods were found at the mouth of the estuary. The estuary integrated residence time is very quick, ranging from 2-5 days. However, T_{res} varies significantly within individual portions of the estuary, and furthermore, for smaller tributaries there are large differences in T_{res} depending on which method of the TEF binning is used (section 3.5), although the estuary integrated values are similar for the two methods.

CHAPTER VI

DISCUSSION

Drivers of Exchange Flow

Although TEF is able to show the full exchange flow, it lacks information about which processes are responsible for the variability. Following MacCready (2011), Chen et al. (2012), and Rayson et al. (2017), the TEF variables are compared with forcing agents in property-property plots (Fig. 14). The tidal volume flux magnitude, defined as

$$Q_{tide} = \langle | \int udA - \langle \int udA \rangle | \rangle, \tag{6.1}$$

represents the strength of the tidal forcing. In Coos Estuary, the tidal scaling Q_{tide} scales linearly with Q_{in}, and is well correlated (r=0.7-0.8) throughout the estuary in the main channel (Fig. 14a), and even more so in South Slough (r=0.87-0.95). Therefore, the exchange flow is dependent on the volume fluxes into the estuary that vary during the spring-neap cycle; as the tidal amplitude and Q_{tide} increases, the volume flux that is incorporated into exchange flow increases. Mechanisms of tidal salt transport are complex and difficult to distinguish, but are typically parameterized as a subtidal dispersive process leading to down gradient salt transport (Wang et al., 2015; MacCready and Geyer, 2009). Common mechanisms include tidal pumping at a constriction (Stommel and Farmer, 1952), tidal trapping due to side embayments (Okubo, 1973; MacVean and Stacy, 2011), shear dispersion (Taylor, 1954), and stirring by eddies (Banas et al., 2004).

Tidal pumping through the constriction at the mouth (i.e. jet-sink flow; Stommel and Farmer, 1952) appears to be the main mechanism for producing exchange flow in the estuary. Tidal asymmetries in velocity and salinity between flood and ebb tide result in a net salt transport into the estuary. During ebb, a

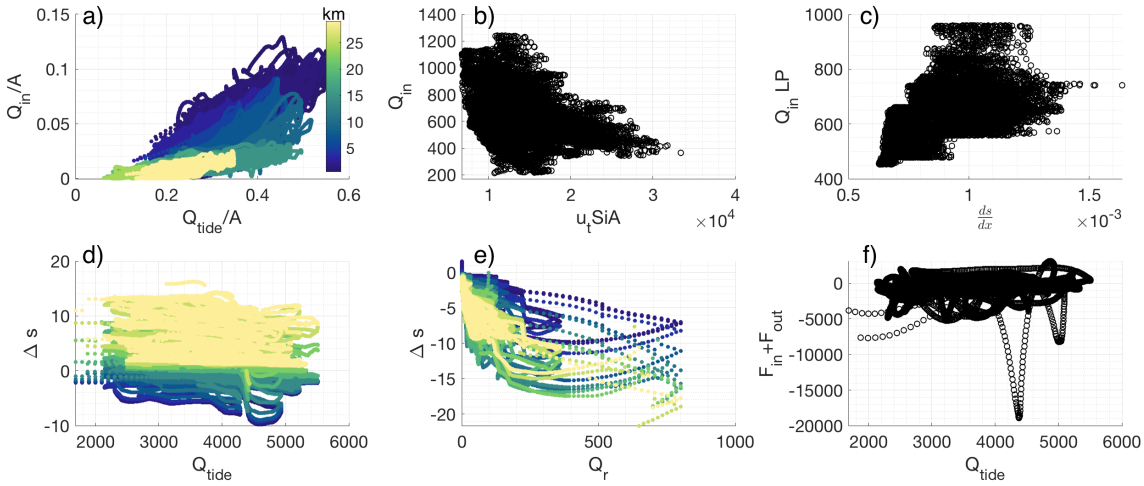

Figure 14. Property-property plots of the TEF variables compared with forcing. The plots colored black are comparisons at the mouth of the estuary, while the colored plots represent cross sections going up estuary, as represented by the colorbar in a) (km). a) Q_{tide} and Q_{in} in the main channel, normalized by the cross sectional area. b) The Simpson number scaling vs Q_{in}. c) Low passed Q_{in} compared with the strength of the horizontal salinity gradient. d) Δs compared with Q_{tide}, showing the relative insensitivity to the spring-neap amplitude, compared to the river discharge Q_r in e). f) shows the net change of salt $F_{in} + F_{out}$ at the mouth of the estuary.

narrow momentum jet carries mixed, lower salinity water out of the estuary. During flood, oceanic water, a majority of which was not affected by the previous ebb tide, radially sinks into the estuary, replacing the outflowing water with oceanic water. Chen et al. (2012) compared the TEF variables to the Stommel and Farmer (1952) mechanism, defining $Q_{prism} = (Q_{tide}/\pi) - (Q_r/2)$, which is the total volume inflow during a tidal cycle. For estuaries where the exchange flow is driven by tidal processes, Q_{prism} represents the upper bound of Q_{in}, whereas in estuaries driven by other processes, the upper bound of the exchange flow would be limited by hydraulic control at the mouth of the estuary. Using this method, it is found that 65% of the tidal prism is converted to exchange flow at the mouth of the estuary by jet-sink flow. Many other dispersive mechanisms for tidal salt transport

are expected to be occurring in the estuary, because of the multiple connecting tributaries, strong velocities, horizontal velocity shear in the along channel velocity, and front formation. However, these are not investigated here.

The Simpson number, $Si = \frac{g\beta\frac{ds}{dx}H^2}{C_D u_t^2}$, represents the strength of the gravitational circulation, where g is gravitational acceleration, β is the coefficient of saline expansion, and C_D is the drag coefficient set to 0.0025. The numerator represents the strength of the baroclinic pressure gradient, and the denominator represents the strength of (bottom boundary) tidal mixing which acts to dampen the gravitational circulation. Here, the Si scaling is compared with the inward volume flux Q_{in} at the mouth of the estuary (Fig. 14b), showing a negligible relationship between the two, consistent with the larger values of Q_{in} during spring tides. Chen et al. (2012) found that the tidal scaling was well representative for exchange flow in the short Merrimack River Estuary, while the Simpson number scaling corresponded well with the exchange flow in the longer Hudson River Estuary. It is expected the seasonal changes in the strength of the baroclinic pressure gradient result in changes in the exchange flow, but that this relationship is masked by the tidal signal. To find this relationship, Q_{in} is low-passed filtered using a loess filter with a half span of 15 days to remove the spring-neap cycle and compared with solely the magnitude of $\frac{ds}{dx}$, as shown in (Fig. 14c). This shows the expected increase in the strength of the exchange flow (at the mouth of the estuary) corresponding with the large seasonal change in the baroclinic pressure gradient; although it is unclear to what degree this influences Q_{in}, as the tidal component dominates the exchange.

The TEF stratification, Δs, is insensitive to the spring-neap cycle (Fig. 14d), but is very sensitive to river discharge (Fig. 14e), in contrast with volume and

salt fluxes throughout the estuary (Fig. 11a). Although the fluxes of salt (F_{in}, F_{out}) in the estuary are in phase with the spring-neap cycle, the net gain of salt $F_{in} + F_{out}$ is not, and is more related to the river discharge (Fig. 11d). These results indicate that the hydrography of the estuary is sensitive to the seasonal changes in Q_r, but because the exchange flow is driven by tidal processes, changes in hydrography are not important for temporal variability of the exchange flow. Banas et al. (2005) showed that tidal diffusion was a density-independent process in Willapa Bay, and we may expect the same for the Coos Estuary. The results presented here with regard to the TEF variables and forcing are very similar to those found for the Columbia River Estuary (MacCready, 2011) and Yaquina Bay (Lemagie and Lerczak, 2015), which are similarly short estuaries with strong tidal forcing.

The large spatial variability of the Eulerian exchange flow, and the large fraction corresponding to tidal fluxes, suggests that the subtidal momentum balance would not be relevant for understanding the exchange flow and that steady estuarine theory (Hansen and Rattray, 1965) would not represent the dynamics of the exchange flow. In estuaries where the length is comparable to the tidal excursion, the baroclinic pressure gradient varies substantially throughout the tidal cycle, reducing the likelihood that the subtidal transport of volume and salinity will be seen in the Eulerian fluxes. In the Coos estuary, the ratio of the salt intrusion compared with the tidal excursion $\frac{L_t}{L_s}$is typically 0.5, roughly half of the Merrimack River estuary (Ralston et al., 2010), but is much shorter than estuaries where the steady fluxes have been shown to be of leading order (e.g. 0.2, Chen et al., 2012). Chen et al. (2012) pointed out there might be a ratio of $\frac{L_t}{L_s}$ that corresponds to a threshold for gravitational circulation (i.e. exchange dominated by the Eulerian component). However, we don't see the transition of the partitioning

of the exchange flow occur as L_s changes throughout the year (Fig. 10d), although it should be noted the the Coos Estuary has a complicated geometry, and the bathymetric transition upstream of 22 km complicate any generalizations.

Implications

The model shows important implications for exchange between the shelf and estuary, as the spring-neap cycle is the dominant time scale for exchange, and the seasonal cycle of exchange flow is not as large as would be expected by the changes in the salt structure of the estuary. These results are in agreement with biological observations in the Coos Estuary: Miller and Shanks (2005) and Roegner and Shanks (2007) documented the importance of the spring-neap cycle for dungeness crab larval transport between the coastal ocean and estuary. These observations give hope that the results found in this study describe the flow and transport of particulates between the estuary and coastal ocean. Adding realistic local wind stress and boundary conditions would better represent the dynamics of the estuary, and would allow examination of the location of source waters that get drawn into the estuary and become a part of the exchange flow.

Giddings and MacCready (2017) used TEF to show how conditions on the shelf affect the exchange flow in the Straight of Juan de Fuca due to reversals of both the baroclinic and barotropic pressure gradients. A similar process is to be expected on the Oregon coast due to sea level set up and set down, as well as a buoyant coastal current found in the winter from rivers south of the Columbia River (Mazzinni et al., 2014) and Columbia River plume intrusions (Hickey and Banas, 2003). However, we may expect this process to be less important in Oregon estuaries due to the reduced importance of baroclinic exchange and the dominance of the tidal exchange. Other estuaries in Oregon, excluding the Columbia River

Estuary, are shallower than the Coos (4-12m), have similar or greater discharge values, and have short horizontal length scales with strong tidal forcing. We expect that these factors cause these estuaries to not be well explained by classic estuarine theory, similar to the Coos Estuary, as the exchange flow and salt fluxes are driven at tidal timescales.

CHAPTER VII

CONCLUSION

A realistic, high resolution, skilled numerical model of the Coos Estuary has been developed and validated. The observations and numerical model show large seasonal, tidal, and spatial variability in hydrography and exchange flow in the Coos Estuary. Using the TEF method, it was found that the estuarine exchange flow is mostly driven by tidal processes, and is strongly modified by the strength of the tidal forcing. Higher exchange of volume and salt throughout the estuary occurs during the larger amplitude fortnightly spring tides, maintaining a persistent exchange flow with constant periodicity year round. The hydrography of the estuary is highly seasonal. The large seasonal changes in hydrography (Sutherland and O'Neil, 2016) are important for changes in stratification, the spatial variation of salinity within the estuary, and the strength of the baroclinic pressure gradient.

The complex geometry of the estuary dictates spatial patterns of salinity, and transport of freshwater throughout the estuary. The main dredged channel is the main pathway for transport of oceanic water as well as river discharge from the largest source of freshwater, which then acts as boundary conditions for the connecting tributaries. Reversals in the along channel salinity gradient and exchange flow persist for synoptic time scales at the mouths of multiple tributaries, likely having important implications for sediment transport in these areas. The short length scale of the estuary, relative to the length of the tidal excursion, limits the applicability of steady estuarine theory. A mechanistic description of the dynamics that drive the total exchange flow in short estuaries with strong tidal forcing is lacking, as the dynamics driving the fluxes of salt occurring at tidal

timescales are complex. The isohaline TEF method provides a robust quantification of the estuarine exchange flow, without resorting to a fully lagrangian framework.

REFERENCES CITED

Banas, N. & Hickey, B. (2005). Mapping exchange and residence time in a model of willapa bay, washington, a branching, macrotidal estuary. *Journal of Geophysical Research: Oceans*, *110*(C11).

Banas, N., Hickey, B., MacCready, P. & Newton, J. (2004). Dynamics of willapa bay, washington: A highly unsteady, partially mixed estuary. *Journal of Physical Oceanography*, *34*(11), 2413–2427.

Banas, N. S., McDonald, P. S. & Armstrong, D. A. (2009). Green crab larval retention in willapa bay, washington: an intensive lagrangian modeling approach. *Estuaries and Coasts*, *32*(5), 893–905.

Burchard, H., Bolding, K., Feistel, R., Gräwe, U., Klingbeil, K., MacCready, P., ... van der Lee, E. M. (2018). The knudsen theorem and the total exchange flow analysis framework applied to the baltic sea. *Progress in Oceanography*.

Caress, D. & Chayes, D. (2008). Mb-system: Open source software for the processing and display of swath mapping sonar data. *Internet: http://www. mbari. org/data/mbsystem*.

Chen, C. (2012). *An unstructured-grid, finite-volume community ocean model: Fvcom user manual*. Sea Grant College Program, Massachusetts Institute of Technology.

Chen, S.-N., Geyer, W. R., Ralston, D. K. & Lerczak, J. A. (2012). Estuarine exchange flow quantified with isohaline coordinates: Contrasting long and short estuaries. *Journal of Physical Oceanography*, *42*(5), 748–763.

Egbert, G. D. & Erofeeva, S. Y. (2002). Efficient inverse modeling of barotropic ocean tides. *Journal of Atmospheric and Oceanic Technology*, *19*(2), 183–204.

Fischer, H. (1972). Mass transport mechanisms in partially stratified estuaries. *Journal of fluid mechanics*, *53*(4), 671–687.

Fischer, H. B. (1976). Mixing and dispersion in estuaries. *Annual review of fluid mechanics*, *8*(1), 107–133.

Geyer, W. R. & MacCready, P. (2014). The estuarine circulation. *Annual Review of Fluid Mechanics*, *46*.

Geyer, W. R. & Nepf, H. (1996). Tidal pumping of salt in a moderately stratified estuary. *Coastal and estuarine studies*, 213–226.

Geyer, W. R., Ralston, D. K. & Holleman, R. C. (2017). Hydraulics and mixing in a laterally divergent channel of a highly stratified estuary. *Journal of Geophysical Research: Oceans*, *122*(6), 4743–4760.

Geyer, W. R., Trowbridge, J. H. & Bowen, M. M. (2000). The dynamics of a partially mixed estuary. *Journal of Physical Oceanography*, *30*(8), 2035–2048.

Giddings, S. & MacCready, P. (2017). Reverse estuarine circulation due to local and remote wind forcing, enhanced by the presence of along-coast estuaries. *Journal of Geophysical Research: Oceans*, *122*(12), 10184–10205.

Giddings, S., MacCready, P., Hickey, B., Banas, N., Davis, K., Siedlecki, S., ... Connolly, T. P. (2014). Hindcasts of potential harmful algal bloom transport pathways on the pacific northwest coast. *Journal of Geophysical Research: Oceans*, *119*(4), 2439–2461.

Hansen, D. V. & Rattray Jr, M. (1965). Gravitational circulation in straits and estuaries.

Hickey, B. M. & Banas, N. S. (2003). Oceanography of the us pacific northwest coastal ocean and estuaries with application to coastal ecology. *Estuaries*, *26*(4), 1010–1031.

Huang, H., Chen, C., Cowles, G. W., Winant, C. D., Beardsley, R. C., Hedstrom, K. S. & Haidvogel, D. B. (2008). Fvcom validation experiments: Comparisons with roms for three idealized barotropic test problems. *Journal of Geophysical Research: Oceans*, *113*(C7).

Jay, D. A. & Smith, J. D. (1990). Circulation, density distribution and neap-spring transitions in the columbia river estuary. *Progress in Oceanography*, *25*(1-4), 81–112.

Knudsen, M. (1900). Ein hydrographischer lehrsatz. *Annalen der Hydrographie und Maritimen Meteorologie*, *28*(7), 316–320.

Largier, J. L. (1992). Tidal intrusion fronts. *Estuaries*, *15*(1), 26–39.

Lemagie, E. P. & Lerczak, J. A. (2015). A comparison of bulk estuarine turnover timescales to particle tracking timescales using a model of the yaquina bay estuary. *Estuaries and coasts*, *38*(5), 1797–1814.

Lerczak, J. A., Geyer, W. R. & Chant, R. J. (2006). Mechanisms driving the time-dependent salt flux in a partially stratified estuary. *Journal of Physical Oceanography*, *36*(12), 2296–2311.

Lerczak, J. A. & Rockwell Geyer, W. (2004). Modeling the lateral circulation in straight, stratified estuaries. *Journal of Physical Oceanography*, *34*(6), 1410–1428.

MacCready, P. (2011). Calculating estuarine exchange flow using isohaline coordinates. *Journal of Physical Oceanography*, *41*(6), 1116–1124.

MacCready, P. & Banas, N. S. (2011). Residual circulation, mixing, and dispersion.

MacCready, P. & Geyer, W. R. (2009). Advances in estuarine physics.

MacCready, P., Rockwell Geyer, W. & Burchard, H. (2018). Estuarine exchange flow is related to mixing through the salinity variance budget. *Journal of Physical Oceanography*(2018).

MacVean, L. J. & Stacey, M. T. (2011). Estuarine dispersion from tidal trapping: a new analytical framework. *Estuaries and Coasts*, *34*(1), 45–59.

Mazzini, P. L., Barth, J. A., Shearman, R. K. & Erofeev, A. (2014). Buoyancy-driven coastal currents off oregon during fall and winter. *Journal of Physical Oceanography*, *44*(11), 2854–2876.

Monismith, S. G., Kimmerer, W., Burau, J. R. & Stacey, M. T. (2002). Structure and flow-induced variability of the subtidal salinity field in northern san francisco bay. *Journal of Physical Oceanography*, *32*(11), 3003–3019.

Murphy, A. H. (1988). Skill scores based on the mean square error and their relationships to the correlation coefficient. *Monthly weather review*, *116*(12), 2417–2424.

Nidzieko, N. J., Hench, J. L. & Monismith, S. G. (2009). Lateral circulation in well-mixed and stratified estuarine flows with curvature. *Journal of Physical Oceanography*, *39*(4), 831–851.

Nidzieko, N. J. & Monismith, S. G. (2013). Contrasting seasonal and fortnightly variations in the circulation of a seasonally inverse estuary, elkhorn slough, california. *Estuaries and coasts*, *36*(1), 1–17.

Nunes, R. & Simpson, J. (1985). Axial convergence in a well-mixed estuary. *Estuarine, Coastal and Shelf Science*, *20*(5), 637–649.

O'Higgins, T. & Rumrill, S. S. (2007). Tidal and watershed forcing of nutrients and dissolved oxygen stress within four pacific coast estuaries: Analysis of time-series data collected by the national estuarine research reserve system-wide monitoring program (2000-2006) within padilla bay (wa), south slough (or), elkhorn slough (ca) and the tijuana river estuary (ca). *Report for the NOAA/UNH Cooperative Institute for Coastal and Estuarine Environmental Technology (CICEET)*, *58*.

Okubo, A. (1973). Effect of shoreline irregularities on streamwise dispersion in estuaries and other embayments. *Netherlands Journal of Sea Research*, *6*(1-2), 213–224.

Peteiro, L. G. & Shanks, A. L. (2015). Up and down or how to stay in the bay: retentive strategies of olympia oyster larvae in a shallow estuary. *Marine Ecology Progress Series*, *530*, 103–117.

Pritchard, D. W. (1956). The dynamic structure of a coastal plain estuary. *J. Mar. Res*, *15*(1), 33–42.

Ralston, D. K., Cowles, G. W., Geyer, W. R. & Holleman, R. C. (2017). Turbulent and numerical mixing in a salt wedge estuary: Dependence on grid resolution, bottom roughness, and turbulence closure. *Journal of Geophysical Research: Oceans*, *122*(1), 692–712.

Ralston, D. K., Geyer, W. R. & Lerczak, J. A. (2010). Structure, variability, and salt flux in a strongly forced salt wedge estuary. *Journal of Geophysical Research: Oceans*, *115*(C6).

Ralston, D. K., Geyer, W. R., Traykovski, P. A. & Nidzieko, N. J. (2013). Effects of estuarine and fluvial processes on sediment transport over deltaic tidal flats. *Continental Shelf Research*, *60*, S40–S57.

Rayson, M. D., Gross, E. S., Hetland, R. D. & Fringer, O. B. (2017). Using an isohaline flux analysis to predict the salt content in an unsteady estuary. *Journal of Physical Oceanography*, *47*(11), 2811–2828.

Roegner, G. C., Needoba, J. A. & Baptista, A. M. (2011). Coastal upwelling supplies oxygen-depleted water to the columbia river estuary. *PloS one*, *6*(4), e18672.

Roegner, G. C. & Shanks, A. L. (2001). Import of coastally-derived chlorophylla to south slough, oregon. *Estuaries*, *24*(2), 244–256.

Scully, M. E., Geyer, W. R. & Lerczak, J. A. (2009). The influence of lateral advection on the residual estuarine circulation: A numerical modeling study of the hudson river estuary. *Journal of Physical Oceanography*, *39*(1), 107–124.

Simpson, J. H., Brown, J., Matthews, J. & Allen, G. (1990). Tidal straining, density currents, and stirring in the control of estuarine stratification. *Estuaries*, *13*(2), 125–132.

Sutherland, D. A., MacCready, P., Banas, N. S. & Smedstad, L. F. (2011). A model study of the salish sea estuarine circulation. *Journal of Physical Oceanography*, *41*(6), 1125–1143.

Sutherland, D. A. & O'Neill, M. A. (2016). Hydrographic and dissolved oxygen variability in a seasonal pacific northwest estuary. *Estuarine, Coastal and Shelf Science*, *172*, 47–59.

Taylor, G. I. (1954). The dispersion of matter in turbulent flow through a pipe. *Proc. R. Soc. Lond. A*, *223*(1155), 446–468.

Umlauf, L. & Burchard, H. (2003). A generic length-scale equation for geophysical turbulence models. *Journal of Marine Research*, *61*(2), 235–265.

Valle-Levinson, A. (2010). *Contemporary issues in estuarine physics*. Cambridge University Press.

Wang, B., Fringer, O., Giddings, S. & Fong, D. (2009). High-resolution simulations of a macrotidal estuary using suntans. *Ocean Modelling*, *26*(1-2), 60–85.

Wang, T., Geyer, W. R., Engel, P., Jiang, W. & Feng, S. (2015). Mechanisms of tidal oscillatory salt transport in a partially stratified estuary. *Journal of Physical Oceanography*, *45*(11), 2773–2789.

Wang, T., Geyer, W. R. & MacCready, P. (2017). Total exchange flow, entrainment, and diffusive salt flux in estuaries. *Journal of Physical Oceanography*, *47*(5), 1205–1220.

Warner, J., Schoellhamer, D., Burau, J. & Schladow, G. (2002). Effects of tidal current phase at the junction of two straits. *Continental Shelf Research*, *22*(11-13), 1629–1642.

Warner, J. C., Geyer, W. R. & Lerczak, J. A. (2005). Numerical modeling of an estuary: A comprehensive skill assessment. *Journal of Geophysical Research: Oceans*, *110*(C5).